

Florida State University Libraries

Electronic Theses, Treatises and Dissertations

The Graduate School

2012

I Was on a Mountain

Daniel William Shafer



THE FLORIDA STATE UNIVERSITY
COLLEGE OF ARTS AND SCIENCES

ISOTOPIC COMPOSITION OF ATMOSPHERIC MERCURY

By

JOHN MICHAEL ROLISON

A Thesis submitted to the
Department of Earth, Ocean, and Atmospheric Science
in partial fulfillment of the
requirements for the degree of
Master of Science

Degree Awarded:
Summer, 2012

John Rolison defended this Thesis on May 31, 2012.

The members of the supervisory committee were:

William M. Landing
Professor Directing Thesis

Vincent Salters
Committee Member

Munir Humayun
Committee Member

The Graduate School has verified and approved the above-named committee members, and certifies that the thesis has been approved in accordance with university requirements.

To Alice

ACKNOWLEDGEMENTS

I would like to thank my advisor, William Landing, for financial and intellectual support during the duration of my time at Florida State University. I would also like to thank my committee members, Vincent Salters and Munir Humayun, for intellectual support and allowing me to unlimited access to the facilities within the Isotope Geochemistry Laboratory at the National High Field Magnetic Laboratory. Nicole Tibbetts was instrumental in my success as an operator of the NEPTUNE. Without the experience and guidance of these individuals this project would not have been a success.

Winston Luke and Mark Cohen with the National Oceanographic and Atmospheric Administration Air Resources Laboratory provided TEKRA data collected in Grand Bay, MS, United States Hg emissions data, and offered their expertise in atmospheric modeling using HYSPLIT. Eric Edgerton and Bud Behgtel provided access and assistance at the OLF site in Pensacola, FL.

Financial support for this research was provided by grants from the National Oceanographic and Atmospheric Administration (NA09OAR4600198 and NA10OAR4600209) and the Electric Power Research Institute (EP-P33676/C15484).

I would also like to thank all of the people I have met in Tallahassee for providing a great environment for living and studying. I want to especially thank Kristina for providing me with the stability, strength, and motivation required for completing graduate school. Above all I want to thank my family for their support and love.

TABLE OF CONTENTS

List of Tables	vi
List of Figures	vii
Abstract	viii
1. INTRODUCTION	1
1.1 Mercury in the Environment	1
1.1.1 Basic Biogeochemical Cycle of Mercury	1
1.1.2 Atmospheric Cycle of Mercury	2
1.2 Introduction to Research Plan	2
2. EXPERIMENTAL METHODS AND FIELD CAMPAIGN	6
2.1 Site Descriptions	6
2.2 Sample collection process	6
2.3 Sample Extraction	7
2.4 Mass Spectrometry	9
3. RESULTS	14
3.1 Collection of $\text{Hg}^0_{(g)}$, $\text{Hg}_{(p)}$, and $\text{Hg}^{\text{II}}_{(g)}$	14
3.2 Hg stable isotope compositions	15
4. DISCUSSION	29
4.1 Mass dependent fractionation of $\text{Hg}^0_{(g)}$	29
4.2 Mass dependent fractionation of $\text{Hg}_{(p)}$ and $\text{Hg}^{\text{II}}_{(g)}$	30
4.3 Mass independent fractionation (MIF)	32
4.3.1 MIF mechanisms	32
4.3.2 MIF in atmospheric Hg	32
4.3.3 Modeling in-aerosol photoreduction	34
4.3.4 MIF of ^{200}Hg and ^{204}Hg	35
4.4 Back-Trajectory Modeling	35
5. CONCLUSIONS	40
APPENDIX	41
APPENDIX 1: SAMPLE COLLECTION INFORMATION FOR THE OLF AND	
GB SITES	41
REFERENCES	47
BIOGRAPHICAL SKETCH	52

LIST OF TABLES

3.1 Replicate analysis of sectioned untreated quartz fiber filters deployed at the OLF site for approximately 72 h.	19
3.2 Isotopic composition of $\text{Hg}^0_{(\text{g})}$ trapped directly in KMnO_4 trapping solution and also the initially trapped on a Au trap before being thermally released and then trapped in KMnO_4 trapping solution.	20
3.3 Isotopic composition of species-specific atmospheric Hg samples collected at Grand Bay, Mississippi (USA) during April-May, 2011.	21
A.1 Sample information for KCl treated quartz fiber filters and untreated quartz fiber filters collected at the OLF site.	42
A.2 Sample information for KCl treated quartz fiber filters and untreated quartz fiber filters collected at the GB site.	45
A.3 Sample information for Au traps collected at the both the Grand Bay and OLF sites.	46

LIST OF FIGURES

1.1	Schematic illustration of the basic biogeochemical Hg cycle (recreated from Selin, 2009).	5
2.1	Site map showing the GB and OLF sites.	11
2.2	Illustration of known Hg emission sources in North America during 2005 (Mark Cohen NOAA/OAR US EPA 2005 National Emissions Inventory Data).	12
2.3	Schematic of extraction system used for QFFs, KCl-QFFs, and gold traps.	13
3.1	(a) Concentration of GEM, RGM, and FPM measured by dual Tekran® 2537A/1130/1135 automated Hg speciation analyzers (Winston Luke NOAA/OAR unpublished data) and (b) mass of Hg collected concurrently on gold traps, KCl treated quartz fiber filters, and untreated quartz fiber filters.	17
3.2	Comparison of average daily concentrations of Hg_p (A) and $Hg^{II}_{(g)}$ (B) as measured by the Tekran® 2537A/1130/1135 automated Hg speciation analyzers and the manual collection method employed for isotope analysis.	18
3.3	^{199}Hg and ^{201}Hg three isotope diagrams for species-specific atmospheric Hg samples collected at Grand Bay, Mississippi (USA) during April-May, 2011.	23
3.4	^{200}Hg and ^{204}Hg three isotope diagrams for species-specific atmospheric Hg samples collected at Grand Bay, Mississippi (USA) during April-May, 2011.	24
3.5	$\Delta^{199}Hg$ (‰) versus $\delta^{202}Hg$ (‰) for atmospheric Hg samples collected at Grand Bay, Mississippi (USA) during April-May, 2011.	25
3.6	$\Delta^{199}Hg$ (‰) versus $\Delta^{201}Hg$ (‰) for atmospheric Hg samples collected at Grand Bay, Mississippi (USA) during April-May, 2011.	26
3.7	$\Delta^{200}Hg$ (‰) versus $\delta^{202}Hg$ (‰) for atmospheric Hg samples collected at Grand Bay, Mississippi (USA) during April-May, 2011.	27
3.8	$\Delta^{200}Hg$ (‰) versus $\Delta^{204}Hg$ (‰) for atmospheric Hg samples collected at Grand Bay, Mississippi (USA) during April-May, 2011.	28
4.1	NOAA HYSPLIT back-trajectory collect for samples on April 25, 2011 (courtesy of Mark Cohen NOAA/ARL unpublished data).	37
4.2	Compilation of back-trajectories on days when $Hg^0_{(g)}$ samples displayed $\delta^{202}Hg$ values ≤ -2 ‰ (courtesy of Mark Cohen NOAA/ARL unpublished data).	38
4.3	Compilation of back-trajectories on days when $Hg^0_{(g)}$ samples displayed $\delta^{202}Hg$ values > -2 ‰ (courtesy of Mark Cohen NOAA/ARL unpublished data).	39

ABSTRACT

The isotopic composition of species-specific atmospheric mercury (Hg) was investigated in the coastal environment of Grand Bay, Mississippi, USA. $\text{Hg}^0_{(\text{g})}$, $\text{Hg}^{\text{II}}_{(\text{g})}$ and $\text{Hg}_{(\text{p})}$ were concurrently separated and collected, and subsequently analyzed for isotopic composition. $\text{Hg}^0_{(\text{g})}$ displayed negative mass dependent fractionation (MDF) with a range $> 3.5\text{‰}$ ($\delta^{202}\text{Hg} = -3.88\text{‰}$ to -0.33‰). $\text{Hg}_{(\text{p})}$ displayed intermediate MDF ($\delta^{202}\text{Hg} = -1.61\text{‰}$ to -0.12‰), while $\text{Hg}^{\text{II}}_{(\text{g})}$ displayed positive MDF ($\delta^{202}\text{Hg} = +0.51\text{‰}$ to $+1.61\text{‰}$). Significant positive mass independent fractionation was observed in $\text{Hg}_{(\text{p})}$ ($\Delta^{199}\text{Hg} = +0.36\text{‰}$ to $+1.36\text{‰}$), while $\text{Hg}^0_{(\text{g})}$ displayed negative MIF ($\Delta^{199}\text{Hg} = -0.41\text{‰}$ to -0.03‰) and $\text{Hg}^{\text{II}}_{(\text{g})}$ displayed intermediate MIF ($\Delta^{199}\text{Hg} = -0.28\text{‰}$ to 0.18‰). Positive MIF of ^{199}Hg and ^{201}Hg measured in $\text{Hg}_{(\text{p})}$ points to significant in-aerosol photoreduction. Significant MIF of ^{200}Hg was observed in all Hg species with $\text{Hg}^0_{(\text{g})}$ displaying negative $\Delta^{200}\text{Hg}$ values of -0.19‰ to -0.06‰ and $\text{Hg}_{(\text{p})}$ and $\text{Hg}^{\text{II}}_{(\text{g})}$ displaying positive $\Delta^{200}\text{Hg}$ values of $+0.06\text{‰}$ to $+0.28\text{‰}$.

CHAPTER ONE

INTRODUCTION

1.1 Mercury in the Environment

1.1.1 Basic Biogeochemical Cycle of Mercury

Mercury (Hg) is a naturally occurring heavy metal with many unique physiochemical properties that contribute to its complex biogeochemical cycle. Being a chalcophilic element, the dominant mineralized form of Hg is cinnabar (HgS). Large deposits of cinnabar are associated with geologic regions characterized by subduction zones and deep-focus earthquakes (Schluter, 2000). A variety of natural and anthropogenic processes release mineralized Hg to the Earth's surface environment. Currently, coal combustion and waste incineration account for the majority of anthropogenic Hg emissions while volcanoes account for the majority of natural emissions (Pacyna *et al*, 2010). At room temperature, elemental Hg (Hg^0) exists as a silvery liquid, which experiences evaporation thereby creating gaseous elemental mercury (GEM; $\text{Hg}^0_{(\text{g})}$). Once GEM has entered the atmosphere it is relatively inert and also relatively insoluble in water, which results in an atmospheric residence time on the order of one year (Schroder and Munthe, 1998). This allows for global-scale transport of $\text{Hg}^0_{(\text{g})}$ emissions in the atmosphere.

Deposition of atmospheric Hg is the primary source of Hg entering aquatic systems (Landis and Keeler, 2002; Hammerschmidt and Fitzgerald, 2006). Once incorporated into aquatic systems inorganic Hg can undergo methylation, thereby creating monomethylmercury (MMHg; CH_3Hg^+). Methylation of Hg in aquatic systems is facilitated by microbial organisms, especially sulfate-reducing bacteria (Gilmour and Henry, 1991). MMHg is the neurologically toxic species of Hg that bioaccumulates and biomagnifies in aquatic and terrestrial ecosystems. The ingestion of wildlife species contaminated with MMHg poses a serious health risk to humans and is currently the principal route of Hg exposure to humans (U.S. EPA, 1997; Fitzgerald and Lamborg, 2005). Figure 1.1 schematically illustrates the basic biogeochemical cycle of Hg.

1.1.2 Atmospheric Cycle of Mercury

In the atmosphere, gaseous elemental Hg (GEM) usually accounts for >95% of the total Hg. This is a result of GEM being volatile and sparingly soluble in water, resulting in a slow removal rate and a long atmospheric residence time. GEM can be oxidized to Hg(II), which has been termed reactive gaseous Hg (RGM). The exact speciation of RGM is still uncertain but can be modeled with some success as Hg halide compounds such as HgCl₂ and HgBr₂. RGM is very soluble in water and is surface reactive, which results in a fast removal rate through wet and dry deposition leading to a short atmospheric residence time of hours to days. Atmospheric Hg also interacts with atmospheric aerosols, resulting in a third atmospheric Hg species, particulate Hg (Hg_(p)). Hg_p has a relatively fast deposition velocity and is scrubbed out of the atmosphere by precipitation. Therefore, Hg_(p) has an atmospheric residence time similar to RGM.

The fate of atmospheric Hg emissions is roughly determined by the speciation of the emission. Local and regional deposition of RGM and Hg_(p) emissions is expected while Hg emitted as GEM will likely be transported over long distances before being oxidized and deposited. Therefore, atmospheric deposition of Hg in urbanized areas possibly consists of anthropogenic Hg derived from local/regional sources as well as the global atmospheric pool of Hg, which is a combination of anthropogenic and natural Hg. Source attribution of Hg deposition in a multi-source environment has proven difficult using available techniques (Lindberg *et al*, 2007).

In light of the observation that Hg in aquatic systems is primarily derived from atmospheric deposition, it is clear that understanding the physical and chemical processes controlling the transport and deposition of atmospheric Hg is of high value. Atmospheric transport and deposition is the key link between atmospheric Hg emissions and the accumulation of Hg in aquatic systems.

1.2 Introduction to Research Plan

Centuries of mining and industrial activities have increased the total amount of Hg cycling through Earth's surface environments, thereby significantly altering its global biogeochemical cycle. Consequently, atmospheric deposition of Hg to the Earth's surface now exceeds pre-industrial deposition by approximately a factor of three (Mason and Sheu, 2002; Fitzgerald *et al.*, 2005). Once deposited to terrestrial or aquatic ecosystems, the potential exists

for conversion to toxic methylmercury, which bioaccumulates and threatens human health through consumption of contaminated organisms (EPA, 1997). Although industrial regulations in many countries now limit the production of products containing Hg and require Hg removal and Hg filter systems to clean atmospheric emissions, such as scrubbers on coal fired power plants, global Hg emissions remain elevated, with Asia accounting for nearly two-thirds of all anthropogenic mercury emissions (Pacyna et al., 2010, Pirrone, et al. 2010).

Our current understanding of the atmospheric cycling of Hg is based on observations of temporal variations in the concentrations of relevant atmospheric Hg species which are gaseous elemental Hg (GEM; $\text{Hg}^0_{(\text{g})}$), gaseous oxidized Hg ($\text{Hg}^{\text{II}}_{(\text{g})}$) compounds and particulate/aerosol bound Hg ($\text{Hg}_{(\text{p})}$). $\text{Hg}^0_{(\text{g})}$ is the dominant form of atmospheric Hg and generally accounts for >95% of total Hg in uncontaminated air (Schroeder and Munthe, 1998; Liu et al., 2010). $\text{Hg}^0_{(\text{g})}$ is highly volatile and only sparingly soluble in water, hence $\text{Hg}^0_{(\text{g})}$ is not efficiently scavenged by wet and dry depositional processes. As a result, the atmospheric residence time of $\text{Hg}^0_{(\text{g})}$ is relatively long, 0.5 to 1 year, which allows for regional/global transport of $\text{Hg}^0_{(\text{g})}$ emissions (Lindberg, 2007). $\text{Hg}^0_{(\text{g})}$ is converted to $\text{Hg}^{\text{II}}_{(\text{g})}$ compounds upon reactions with atmospheric oxidants, such as halogens, ozone, and OH (Lin and Pehkonen, 1999; Holmes et al., 2009; Subir et al. 2011). Because $\text{Hg}^{\text{II}}_{(\text{g})}$ is highly reactive and water soluble, local/regional deposition is expected in the vicinity of direct $\text{Hg}^{\text{II}}_{(\text{g})}$ emission sources. $\text{Hg}^{\text{II}}_{(\text{g})}$, and to a lesser extent $\text{Hg}^0_{(\text{g})}$, can become associated with aerosols and particulate matter to make $\text{Hg}_{(\text{p})}$, which is also effectively removed from the atmosphere through wet and dry deposition. Therefore, both wet and dry deposition of atmospheric Hg is dominated by oxidized Hg species (Schroeder and Munthe, 1998; Guentzel et al., 2001).

Oxidized Hg species (i.e. $\text{Hg}^{\text{II}}_{(\text{g})}$ and $\text{Hg}_{(\text{p})}$) are typically present in the atmosphere at concentrations $<10 \text{ pg/m}^3$ in uncontaminated rural environments but can reach levels in excess of 300 pg/m^3 in contaminated industrial areas and during atmospheric Hg depletion events (Sprovieri et al., 2002; Lindberg et al., 2002; Liu et al., 2010). $\text{Hg}^{\text{II}}_{(\text{g})}$ and $\text{Hg}_{(\text{p})}$ can account for a significant fraction of total atmospheric Hg emissions during industrial processes such as municipal waste incineration and fossil fuel combustion (Capri, 1996; Pirrone et al., 2001). Coal fired power plant plumes can transport direct emissions of $\text{Hg}^{\text{II}}_{(\text{g})}$ compounds over distances greater than 100 km (Edgerton et al., 2006). Accordingly, elevated wet and dry deposition rates around large urban/industrial centers are expected and were observed during the Lake Michigan

Mass Balance Study (Keeler and Landis, 2002). Furthermore, Landis et al. (2005) observed increasing levels of $\text{Hg}^{\text{II}}_{(\text{g})}$ with altitude in the marine troposphere off the Atlantic coast of Florida, indicating oxidation of $\text{Hg}^0_{(\text{g})}$ at high altitude. Guentzel et al. (2001) hypothesized that tall (12-16 km) convective thunderstorms in Florida during the wet season can scavenge high altitude $\text{Hg}^{\text{II}}_{(\text{g})}$ and $\text{Hg}_{(\text{p})}$, thereby enhancing deposition rates. Source attribution of Hg deposition on a regional scale is challenging using concentration and speciation data only. This is because $\text{Hg}^0_{(\text{g})}$ may be deposited, upon oxidation, far from its emission source(s), while direct $\text{Hg}^{\text{II}}_{(\text{g})}$ and $\text{Hg}_{(\text{p})}$ emissions will be deposited relatively close to emission sources. Therefore, deposition on a regional scale potentially represents a combination of multiple sources of Hg (global, regional, or local; natural or anthropogenic). Hg isotope ratio measurements could provide a valuable new tool for identifying sources of Hg deposition in a multiple source environment.

Over the last decade, development and implementation of analytical methods to precisely measure Hg isotope ratios have documented mass dependent fractionation (MDF) of Hg isotopes during a variety of natural and industrial Hg transformations (Smith et al., 2005; Bergquist and Blum, 2007; Kritee et al., 2007, 2008, 2009; Zheng et al., 2007; Estrade et al., 2009; Laffont et al., 2009; Sonke et al., 2010). Additionally, the discovery of mass independent fractionation (MIF) of Hg isotopes has been documented during photochemical and non-photochemical abiotic reduction (Bergquist and Blum, 2007; Zheng and Hintelmann, 2009, 2010b), and physical (Estrade et al., 2009) and chemical processes (Wiederhold et al., 2010). Such processes lead to differences in the Hg isotopic composition of different emission sources, both natural and anthropogenic. Therefore, Hg isotope ratios measured in ambient air could be used to trace the source of Hg. However, atmospheric processes (i.e. transportation, oxidation/reduction, deposition, reemission) could induce additional Hg isotope fractionation, thereby changing the Hg isotopic composition relative to the source.

This study reports an initial attempt to measure the isotopic compositions of $\text{Hg}^0_{(\text{g})}$, $\text{Hg}^{\text{II}}_{(\text{g})}$, and $\text{Hg}_{(\text{p})}$ collected concurrently in a coastal marine environment. The objectives of this work are 1) to establish methods to separate and collect $\text{Hg}^0_{(\text{g})}$, $\text{Hg}^{\text{II}}_{(\text{g})}$, and $\text{Hg}_{(\text{p})}$ of sufficient quantity for isotope ratio analysis, 2) characterize the isotopic composition of $\text{Hg}^0_{(\text{g})}$, $\text{Hg}^{\text{II}}_{(\text{g})}$, and $\text{Hg}_{(\text{p})}$, and 3) use the isotopic composition of $\text{Hg}^0_{(\text{g})}$, $\text{Hg}^{\text{II}}_{(\text{g})}$, and $\text{Hg}_{(\text{p})}$ to identify the dominant atmospheric sources and cycling process for Hg.

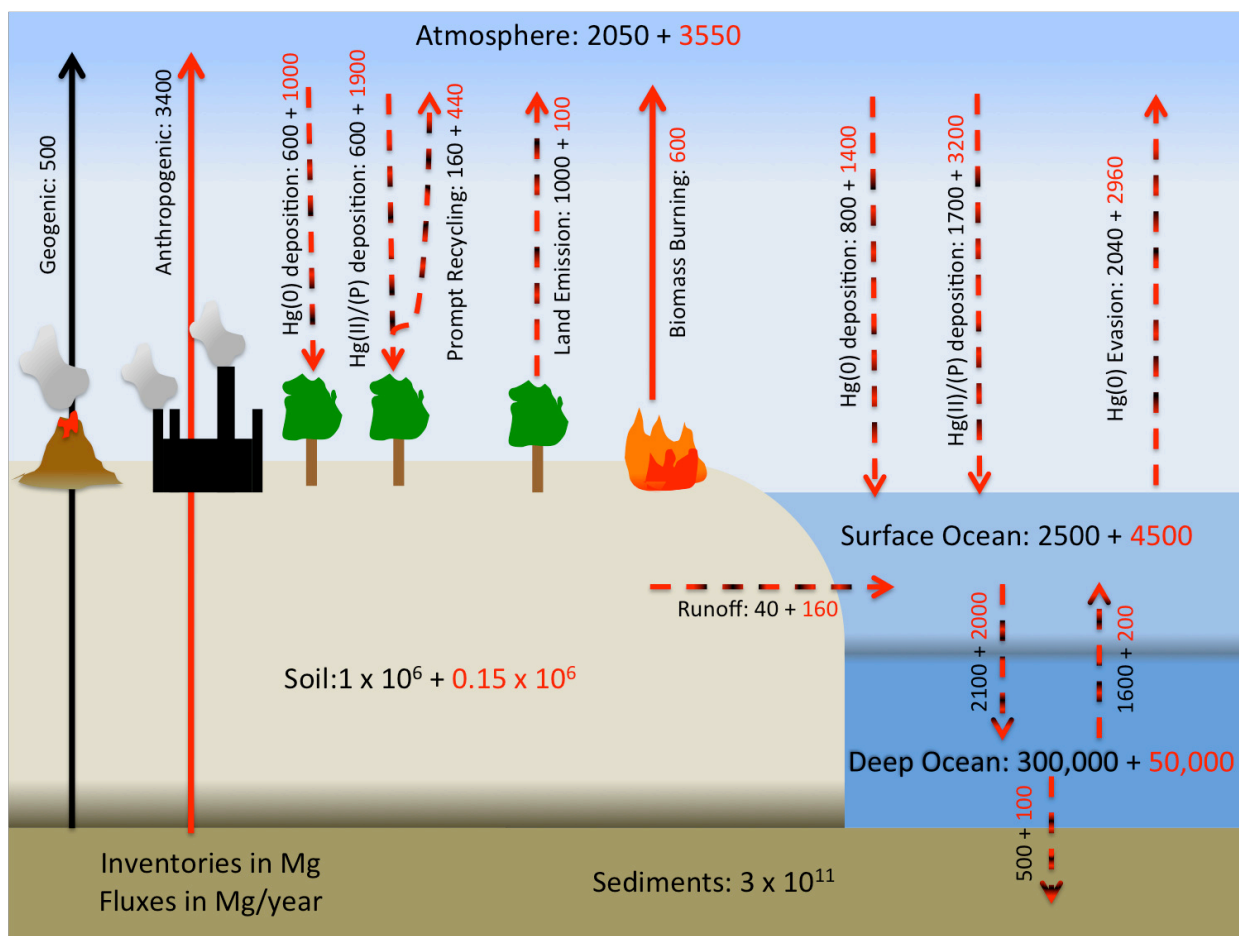


Figure 1.1: Schematic illustration of the basic biogeochemical Hg cycle (recreated from Selin, 2009). Natural (preindustrial) fluxes [megagrams (Mg) year⁻¹] and inventories, in Mg, are noted in black. Anthropogenic contributions are in red. Red-and-black dashed lines note natural fluxes augmented by anthropogenic activities.

CHAPTER TWO

EXPERIMENTAL METHODS AND FIELD CAMPAIGN

2.1 Site descriptions

Daily atmospheric Hg samples were collected during a three-week field campaign (18 April 2011 to 9 May 2011) at the Grand Bay National Estuarine Research Reserve in Moss Point, MS. (Lat: 30.41°N - Long: 88.40°W) (Figure 2.1). Grand Bay (GB) is situated on the northern coast of the Gulf of Mexico and is often influenced by air masses coming from the marine environment, especially during the summer months. The GB site is semi-rural, surrounded by a sparsely populated suburban area. Possible local anthropogenic atmospheric Hg emission sources include a large oil refinery 10 km to the SW with an unknown Hg emission inventory and the Victor J. Daniel Jr. Electric Generating Plant approximately 25 km to the NW. Other regional and continental anthropogenic Hg emission sources are illustrated in figure 2.2. A large open field within the reserve, 5 km NW of the Gulf of Mexico, was selected as the site to deploy atmospheric sampling equipment.

Aerosol samples were also collected at a second site located 21 km NW of Pensacola, FL and 20 km N of the Gulf of Mexico (Lat: 30.55°N. Long: 87.38°W). The site, termed Outlying Landing Field (OLF), is located on the edge of large open field and is considered suburban. Plant Crist, a coal fired electrical facility, is located 15 km ENE of the site and is considered to be the dominant local source of atmospheric Hg emissions (Caffrey et al., 2010).

Figure 2.2 illustrates the known Hg emissions in North America during the year 2005.

2.2 Sample collection process

$\text{Hg}^{\text{II}}_{(\text{g})}$ and $\text{Hg}_{(\text{p})}$ were collected using a Tisch 5170V-BL high volume aerosol sampler (Tisch Environmental Inc., Ohio, USA). The system is equipped with a vacuum pump that creates a flow across the filter interface of approximately 3 L/cm²-min. The area of the filter interface is approximately 406 cm², resulting in a total flow of 1.2 m³/min (± 0.1 m³/min). The total flow rate is dependent upon temperature, barometric pressure, and vacuum pressure behind the filter. $\text{Hg}_{(\text{p})}$ was collected on untreated quartz fiber filters (Whatman QM-A). $\text{Hg}^{\text{II}}_{(\text{g})}$ was collected on quartz fiber filters treated with potassium chloride (KCl, Fisher Scientific, >99.9%). Treatment consisted of soaking the quartz fiber filters in 10% KCl (w/v, 1.34 M) solution until

fully saturated at which time they were removed and allowed to air dry under a laminar flow hood. Untreated and KCl treated quartz fiber filters (QFF and KCl-QFF) were pre-combusted at 550 °C for ≥ 10 hours to eliminate any trace of Hg prior to use. Immediately following pre-combustion, the filters were wrapped in pre-baked aluminum foil and then placed inside a sealed, clean plastic bag. The filters were deployed in a filter cartridge that was mounted to the top of the aerosol sampler. After deployment, the filters were removed from the filter cartridge, placed back in the aluminum foil and plastic bag, and were kept frozen until further processing.

At the GB site, untreated and treated QFFs were deployed simultaneously as a filter stack, in a single filter cartridge, for an interval of approximately 24 hours. This allowed for collection of sufficient quantities of $\text{Hg}_{(\text{p})}$ and $\text{Hg}^{\text{II}}_{(\text{g})}$ required for isotope analyses (~ 3 ng Hg). The untreated QFF, on top of the stack, collected $\text{Hg}_{(\text{p})}$ while $\text{Hg}^{\text{II}}_{(\text{g})}$ was transmitted and collected on the KCl-QFF on the bottom of the stack. Thus, $\text{Hg}_{(\text{p})}$ and $\text{Hg}^{\text{II}}_{(\text{g})}$ were collected separately from the same air mass. At the OLF site, untreated QFFs only were deployed during August 2010 for 72-hour intervals. Deploying the filters longer resulted in more Hg being collected. Therefore, these filters were sectioned into thirds and subsequently extracted and analyzed as individual samples.

$\text{Hg}^0_{(\text{g})}$ was collected and pre-concentrated using gold (Au) traps via gold-mercury amalgamation. Gold traps consisted of approximately 1 g of gold-coated sand secured in a quartz tube with quartz wool. Each gold trap was cleaned of residual Hg by baking at 500 °C for one hour and then stored in a sealed glass test tube until use. A vacuum pump was used to pull air through the gold trap at approximately 2 L/min for 24-hour intervals. The gold traps were deployed approximately 2 m above ground level. Since a pre-filter was not employed, gold traps collected Hg_T ($\text{Hg}^0_{(\text{g})}$, $\text{Hg}^{\text{II}}_{(\text{g})}$, and $\text{Hg}_{(\text{p})}$) rather than $\text{Hg}^0_{(\text{g})}$ solely. However, the ambient concentration of $\text{Hg}^0_{(\text{g})}$ was typically 2-3 orders of magnitude higher than $\text{Hg}^{\text{II}}_{(\text{g})}$ and $\text{Hg}_{(\text{p})}$ during the field campaign. Therefore, the contribution of $\text{Hg}^{\text{II}}_{(\text{g})}$ and $\text{Hg}_{(\text{p})}$ to the total Hg sampled by the gold trap is negligible. Gold trap Hg samples will be referred to as $\text{Hg}^0_{(\text{g})}$ in the following discussion.

2.3 Sample extraction

Figure 2.3 illustrates the Hg combustion system used for extraction of Hg from gold traps and QFFs (untreated and treated). The quartz tubes (OD 2.54 cm; ID 2.44 cm; length 61 cm)

were fitted with threaded Teflon end caps used to connect the quartz tube to a supply of ultra high purity Ar and O₂ carrier gases and a Teflon impinger (30 mL microcolumn; 6.4 mm ID x 9.6 mm OD x 25 cm capillary; Savillex, Minnesota, USA) via Teflon tubing. The carrier gases were passed through gold traps to remove any trace Hg. Quartz tubes and Teflon connectors were cleaned by soaking in a 8 M HNO₃ solution for ≥ 48 h and rinsed thoroughly with high purity DI (18.2 M Ω .cm) water.

Quartz tubes loaded with gold traps and QFFs were heated in a Lindberg/Blue M Mini-Mite programmable tube furnace. Hg_P on uncoated QFFs was liberated and volatilized using a multi-step heating routine. The first heating step ramped the temperature to 500° C at 50 °C/min, the temperature then ramped to 800 °C at 25 °C/min. The temperature was then held at 800 °C for 15 min before cooling to room temperature. Volatilized Hg was transported out of the quartz tube in a stream of Ar (35 mL/min) and O₂ (15 mL/min) and was then captured in a KMnO₄ trapping solution. O₂ was used as a carrier gas during combustion of untreated QFFs to ensure that oxidation of any organic matter was complete. Gold traps and KCl-QFFs were extracted using the same combustion method with the only differences being a lower maximum temperature and the lack of O₂ as a carrier gas. Instead of using a mixed Ar/O₂ carrier gas, Ar was used solely at a flow rate of 50 mL/min. Both sample types were heated to 500 °C at 50 °C/min, held for 20 min at 500 °C, and then allowed to cool to room temperature. KCl melts at 771 °C and Rutter et al. (2008) reported evaporation and condensation of KCl at temperatures lower than 771 °C in a similar combustion system using KCl treated quartz fiber filters. Also, heating gold traps and KCl-QFFs to temperatures above 500 °C did not release additional Hg. Thus, 500 °C was chosen as the maximum temperature for both sample types.

During combustion, volatilized Hg is primarily in the Hg⁰_(g) state. Therefore, a strong oxidizing agent, such as potassium permanganate (KMnO₄), is required for trapping. During combustion, the carrier gas enters the impinger and is introduced to the trapping solution at which time gaseous Hg⁰ is oxidized to Hg^{II} and is trapped in the solution. Different concentrations of KMnO₄ were tested to determine the optimal trapping solution. Using a cold vapor atomic fluorescence spectrometer (Model II, Brooks Rand Labs, Washington, USA) in conjunction with a gold trap, a 2.5 mM KMnO₄ in 1.13 M HNO₃ solution was deemed adequate because >99% trapping efficiency was achieved during elemental Hg vapor injections and combustion of standard reference materials (NIST SRM 1572), while minimizing the Hg blank

associated with KMnO_4 . The addition of O_2 helped the KMnO_4 solution retain its oxidizing efficiency by oxidizing gases evolved during combustion that would otherwise be oxidized by the KMnO_4 solution. In the absence of O_2 , combustion of heavily loaded QFFs consumed the KMnO_4 before the combustion routine was complete. O_2 was deemed unnecessary during combustion of gold traps and KCL-QFFs because both sample types contained significantly less organic matter and therefore the trapping efficiency of the KMnO_4 solution was not compromised. Breakthrough of Hg during sample extractions, monitored via CV-AFS, was negligible (<20 pg).

2.4 Mass spectrometry

Hg standards and extracted samples were analyzed for Hg concentrations and isotope compositions using a cold-vapor introduction system interfaced to a multi-collector inductively coupled plasma mass spectrometer (CV-MC-ICP-MS). A CETAC HGX-200 continuous flow cold-vapor (CV) generator was coupled to a Thermo Finnigan Neptune MC-ICP-MS. Dissolved Hg^{II} was reduced by online mixing of 0.16 M SnCl_2 in 1.2 M HCl with the sample solution, generating a continuous flow of $\text{Hg}^0_{(\text{g})}$. The flow rates of the sample solution and SnCl_2 solution were both approximately 0.8 mL/min. All standards and samples were partially reduced with 0.004 mL of 0.72 M $\text{NH}_2\text{OH}\cdot\text{HCl}$ per 1 mL of 2.5 mM KMnO_4 to dissolve manganese oxides immediately prior to analysis. Drift in instrumental mass bias was corrected for using the standard-sample-standard bracketing technique. The international delta-0 Hg standard, NIST SRM 3133, was employed as the bracketing standard. Bracketing standards were matrix matched and concentration matched to within 10% of all samples analyzed. Mass limitations of samples restricted data acquisition time to 4 min (1 block, 60 cycles, 4 s integrations). After each analysis the introduction system was washed with 1.14 M HNO_3 until signal intensity on ^{202}Hg achieved blank signal (≤ 0.005 V). Blank signals were always $\leq 1\%$ of sample signals. Standard operating conditions were optimized daily for signal intensity and stability.

Hg isotope compositions are reported using the standard delta (δ) notation (Blum and Bergquist, 2007):

$$\delta^{xxx}\text{Hg} = \left[\frac{R_{\text{sample}}^{xxx/198}}{R_{\text{NIST 3133}}^{xxx/198}} - 1 \right] * 1000\text{‰} \quad (1)$$

where xxx = 199, 200, 201, 202, 204. Any isotope composition that does not follow theoretical mass dependent fractionation (MDF) is considered an isotope anomaly caused by mass independent fractionation (MIF). MIF is reported using the “capital delta” (Δ) notation as the difference between the measured and the theoretical MDF value (Blum and Bergquist, 2007):

$$\Delta^{199}\text{Hg} (\text{‰}) = \delta^{199}\text{Hg} - (\delta^{202}\text{Hg} \times 0.252) \quad (2)$$

$$\Delta^{200}\text{Hg} (\text{‰}) = \delta^{200}\text{Hg} - (\delta^{202}\text{Hg} \times 0.502) \quad (3)$$

$$\Delta^{201}\text{Hg} (\text{‰}) = \delta^{201}\text{Hg} - (\delta^{202}\text{Hg} \times 0.752) \quad (4)$$

$$\Delta^{204}\text{Hg} (\text{‰}) = \delta^{204}\text{Hg} - (\delta^{202}\text{Hg} \times 1.493) \quad (5)$$

A secondary reference material, UM-Almadén Hg standard, was analyzed during each analytical session to quantify the analytical reproducibility of CV-MC-ICP-MS isotope ratio analysis. It was prepared in an identical KMnO_4 matrix and at concentrations similar to sample solutions. During the analysis period (May-Oct 2011) the UM-Almadén standard averaged $\delta^{202}\text{Hg} = -0.66\text{‰} \pm 0.09\text{‰}$ (2SD, n = 30), $\Delta^{199}\text{Hg} = -0.01\text{‰} \pm 0.07\text{‰}$ (2SD, n = 30), and $\Delta^{201}\text{Hg} = -0.04\text{‰} \pm 0.07\text{‰}$ (2SD, n = 30) (Table 3.2), which is consistent with values reported by other laboratories (Blum and Bergquist, 2007). Additionally, procedural replicates of QFFs collected at the OLF site were analyzed for Hg isotope composition, as were gold traps loaded with an elemental Hg vapor standard. Analytical uncertainties are reported as the larger value of either 2SD of the reproducibility of the UM-Almadén standard or 2SD of procedural replicates.

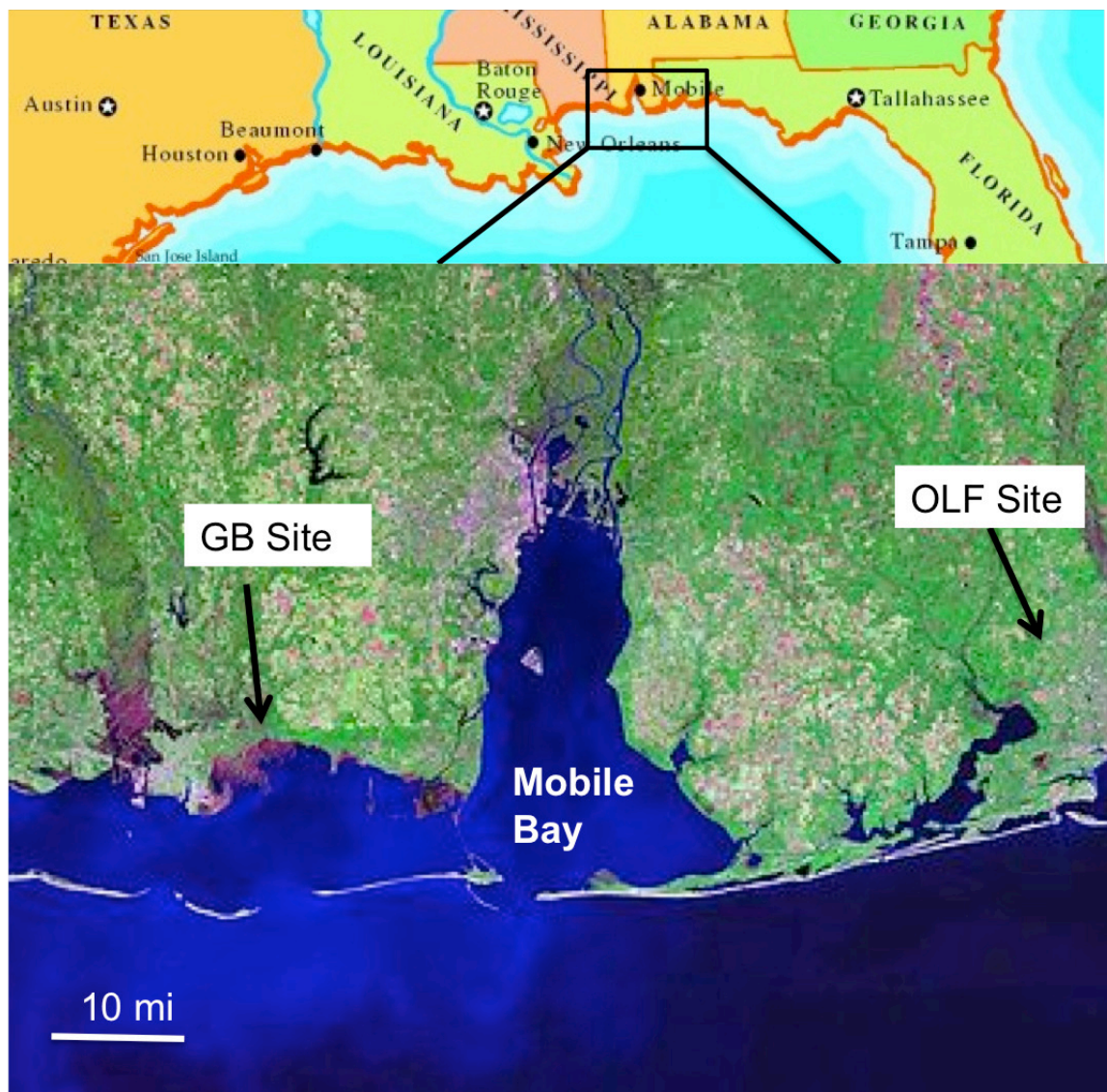


Figure 2.1: Site map showing the GB and OLF sites.

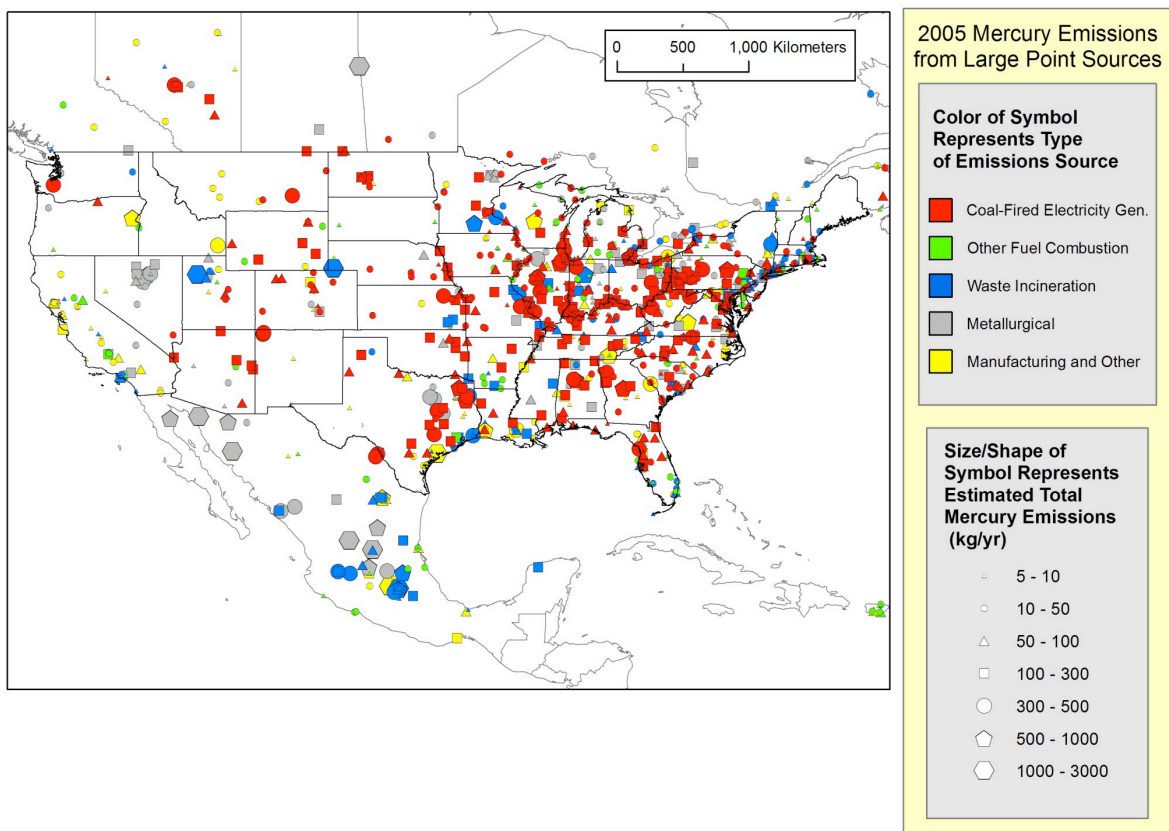


Figure 2.2: Illustration of known Hg emission sources in North America during 2005 (Mark Cohen NOAA/OAR US EPA 2005 National Emissions Inventory Data).

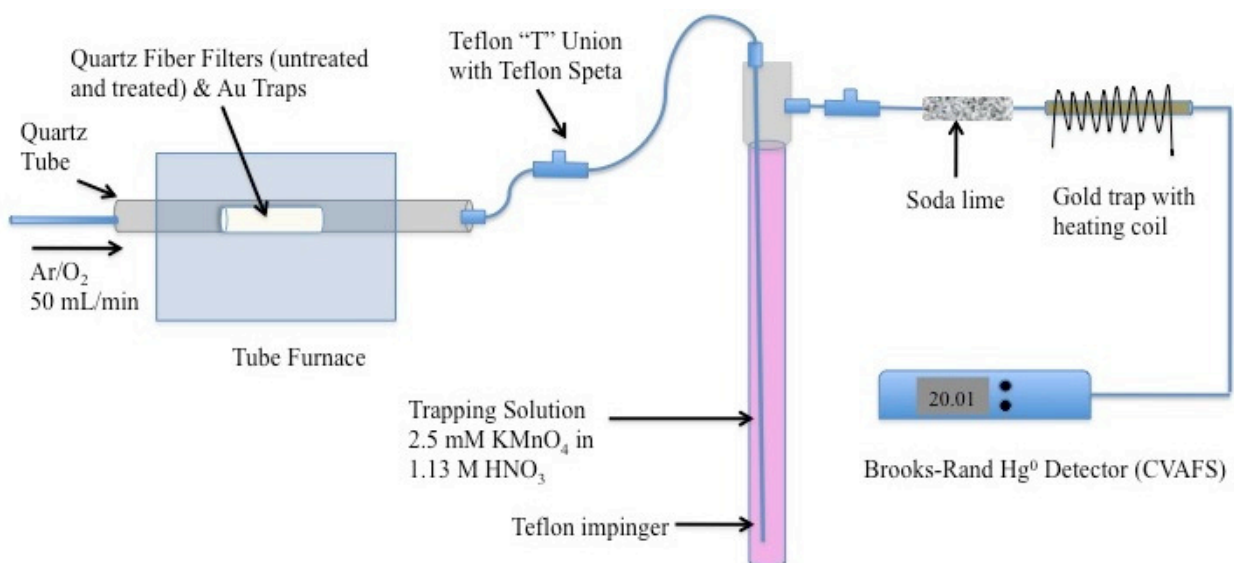


Figure 2.3: Schematic of extraction system used for QFFs, KCl-QFFs, and gold traps.

CHAPTER THREE

RESULTS

3.1 Collection of $\text{Hg}^0_{(\text{g})}$, $\text{Hg}_{(\text{p})}$, and $\text{Hg}^{\text{II}}_{(\text{g})}$

The effectiveness of KCl treated quartz filters at capturing $\text{Hg}^{\text{II}}_{(\text{g})}$ in this study was evaluated by comparison with hourly integrated $\text{Hg}^{\text{II}}_{(\text{g})}$ concentration measurements made with two collocated Tekran[®] 2537A/1130/1135 automated Hg speciation units operating asynchronously to provide continuous mercury species measurements (operated by W. Luke, NOAA/Air Resources Laboratory). Rutter et al. (2008) previously concluded that manual KCl-QFFs techniques and Tekran[®] speciation units compare well in terms of quantifying $\text{Hg}^{\text{II}}_{(\text{g})}$. The Tekran[®] unit uses a KCl-coated annular denuder to collect $\text{Hg}^{\text{II}}_{(\text{g})}$ species which are collectively operationally defined as reactive gaseous Hg (RGM) (Landis et al. 2002). Fine particulate Hg (FPM; particle size < 2.5 μm) was collected on a particulate filter and gaseous elemental Hg (GEM) was collected on an internal gold trap.

During the initial phase the field campaign (18 April - 27 April), RGM at GB did not reach concentrations above 10 pg/m^3 and 24 h averages were typically $\leq 1 \text{ pg}/\text{m}^3$ (Fig. 3.1a). Consequently, daily KCl-QFFs deployed during this time interval were loaded with < 2 ng Hg per filter and precise isotope ratio measurements were not possible. During the final phase of the field campaign (28 April - 9 May), RGM concentrations were elevated and displayed a strong diurnal cycle typical of the marine environment (Laurier et al. 2003; Holmes et al., 2009) with a maximum peak of $\sim 70 \text{ pg}/\text{m}^3$ and 24 h averages $\geq 5 \text{ pg}/\text{m}^3$ (Fig. 3.1a). Daily KCl-QFFs deployed during this time interval were, on average, loaded with > 5 ng Hg per filter (Fig 3.1b).

GEM concentrations averaged 1.5 ng/m^3 over the duration of the field campaign (Fig. 3.1a). Daily gold traps, on average, were loaded with 3.3 ng of Hg. One gold trap was deployed for approximately 48 h (26 April - 28 April) and was loaded with 11 ng of Hg. The FPM concentration shows a similar pattern as RGM, with increased concentrations and a strong diurnal cycle during the final phase of the field campaign (Fig. 3.1a). Daily QFFs collected during the final phase of the field campaign were, on average, loaded with > 5 ng of Hg.

Average daily concentrations of Hg_{p} and $\text{Hg}^{\text{II}}_{(\text{g})}$ were calculated for the filter based manual collection method using the aerosol sampler flow rate which was monitored during the

collection periods by measuring the vacuum pressure under the filters and the ambient temperature and atmospheric pressure. The flow rate of the aerosol sampler was on average 1.2 m³/min with a variation of approximately 0.1 m³/min due to the filters becoming loaded and changes in temperature and atmospheric pressure. Average daily concentrations of FPM and RGM as measured by the Tekran[®] 2537A/1130/1135 automated Hg speciation units were calculated by averaging the data over the time interval represented by the manual collected filter samples. Figure 3.2a displays the daily averages of Tekran[®] FPM versus the uncoated QFFs Hg_p (slope = 0.33 ± 0.07; y-intercept = 0.46 ± 0.60) and Figure 3.2b displays the daily averages of Tekran[®] RGM versus KCl-QFFs Hg^{II}_(g) (slope = 0.35 ± 0.06; y-intercept = 0.53 ± 0.55). The two methods show reasonable agreement but the manual collection method consistently results in lower average daily concentrations. This may be partially due to the fact that the filters were collected at ground level in a highly vegetated area while the Tekran[®] instrument was located on the open coast and installed on a tower with an elevation of approximately 10m. Deposition of Hg_p and Hg^{II}_(g) onto vegetated surfaces may be significant around the filter collection site which would result in decreased concentrations.

Procedural blanks of gold traps and filters were collected and analyzed for Hg content by CV-AFS. Blank gold traps averaged ≤ 50 pg of Hg (n=3) while field blanks for QFFs and KCl-QFFs averaged ≤ 200 pg of Hg (n=3).

3.2 Hg stable isotope compositions

The Hg isotope compositions of replicate extractions and analysis of the OLF QFF filters are reported in Table 3.1. The averages of the 2SD calculated for each set of three samples were used to approximate the reproducibility of the entire method for collection, extraction and isotope ratio analysis for QFFs and KCl-QFFs. The reproducibility of Hg isotope compositions of gold traps loaded with an elemental Hg vapor in equilibrium with liquid elemental Hg (Fisher Mercury Metal Redistilled) is reported in Table 3.2. It is clear that the process of desorbing the gold traps is not inducing isotope fractionation. These uncertainties are applied to all samples accordingly unless the 2SD of the reproducibility of the UM-Almadén standard is larger.

The isotopic compositions for samples collected at GB during the field campaign are summarized in Table 3.3. Hg⁰_(g) displayed the lowest δ²⁰²Hg and a range of > 3.5‰ (-3.88‰ ± 0.13‰ to -0.33‰ ± 0.13‰, 2SD). Hg_(p) displayed intermediate δ²⁰²Hg values (-1.61‰ ± 0.16 to

-0.12‰ ± 0.16, 2SD) and $\text{Hg}^{\text{II}}_{(\text{g})}$ displayed the highest $\delta^{202}\text{Hg}$ values (+0.51‰ ± 0.16 to +1.61‰ ± 0.16, 2SD). Three-isotope diagrams of $\delta^{202}\text{Hg}$ vs $\delta^{199}\text{Hg}$, $\delta^{200}\text{Hg}$, and $\delta^{201}\text{Hg}$, and $\delta^{201}\text{Hg}$ reveal significant mass-independent fractionation (MIF) (Fig. 3.3 and 3.4). $\text{Hg}_{(\text{p})}$ is characterized by significant positive $\Delta^{199}\text{Hg}$ and $\Delta^{201}\text{Hg}$ ($\Delta^{199}\text{Hg}$ = +0.36‰ ± 0.07‰ to +1.36‰ ± 0.07‰, 2SD; $\Delta^{201}\text{Hg}$ = +0.30‰ ± 0.08‰ to +1.20‰ ± 0.08‰, 2SD), while $\text{Hg}^0_{(\text{g})}$ and $\text{Hg}^{\text{II}}_{(\text{g})}$ display negative $\Delta^{199}\text{Hg}$ and $\Delta^{201}\text{Hg}$ values or values that are indistinguishable from zero, with the exception of KCl-QFF 05/07-05/08 ($\Delta^{199}\text{Hg}$ = 0.18‰ ± 0.07, 2SD; $\Delta^{201}\text{Hg}$ = 0.19‰ ± 0.08, 2SD) (Fig. 3.5). A linear regression of $\Delta^{199}\text{Hg}$ and $\Delta^{201}\text{Hg}$ for all samples yields a slope of 1.15 ± 0.02 (r^2 = 0.99) (Fig. 3.6).

Significant MIF of ^{200}Hg was recently reported in atmospheric Hg in the Great Lakes regions of the U.S., Florida, and Canada, including precipitation and $\text{Hg}^0_{(\text{g})}$ (Chen et al, 2012; Gratz et al., 2010; Sherman et al, 2012). Atmospheric Hg at GB also displayed significant MIF of ^{200}Hg (Fig. 3.7). $\text{Hg}^0_{(\text{g})}$ was characterized by negative $\Delta^{200}\text{Hg}$ = -0.19‰ ± 0.06‰ to -0.06‰ ± 0.06‰ (2SD). $\text{Hg}^{\text{II}}_{(\text{g})}$ and $\text{Hg}_{(\text{p})}$ displayed positive $\Delta^{200}\text{Hg}$ of similar magnitude ($\text{Hg}^{\text{II}}_{(\text{g})}$ $\Delta^{200}\text{Hg}$ = +0.08‰ ± 0.06‰ to +0.28‰ ± 0.06‰, 2SD; $\text{Hg}_{(\text{p})}$ $\Delta^{200}\text{Hg}$ = +0.06‰ ± 0.06‰ to +0.26‰ ± 0.06‰, 2SD).

Significant MIF of ^{204}Hg was also observed in the samples collect at GB (Table 3.3 and Figure 3.8). $\text{Hg}^0_{(\text{g})}$ displayed a range of $\Delta^{204}\text{Hg}$ = -0.37‰ ± 0.22‰ to 0.15‰ ± 0.22‰ (2SD). $\text{Hg}^{\text{II}}_{(\text{g})}$ and $\text{Hg}_{(\text{p})}$ displayed negative $\Delta^{204}\text{Hg}$ of similar magnitude ($\text{Hg}^{\text{II}}_{(\text{g})}$ $\Delta^{204}\text{Hg}$ = -0.41‰ ± 0.14‰ to 0.31‰ ± 0.14‰, 2SD; $\text{Hg}_{(\text{p})}$ $\Delta^{204}\text{Hg}$ = -0.84‰ ± 0.22‰ to -0.09‰ ± 0.22‰, 2SD).

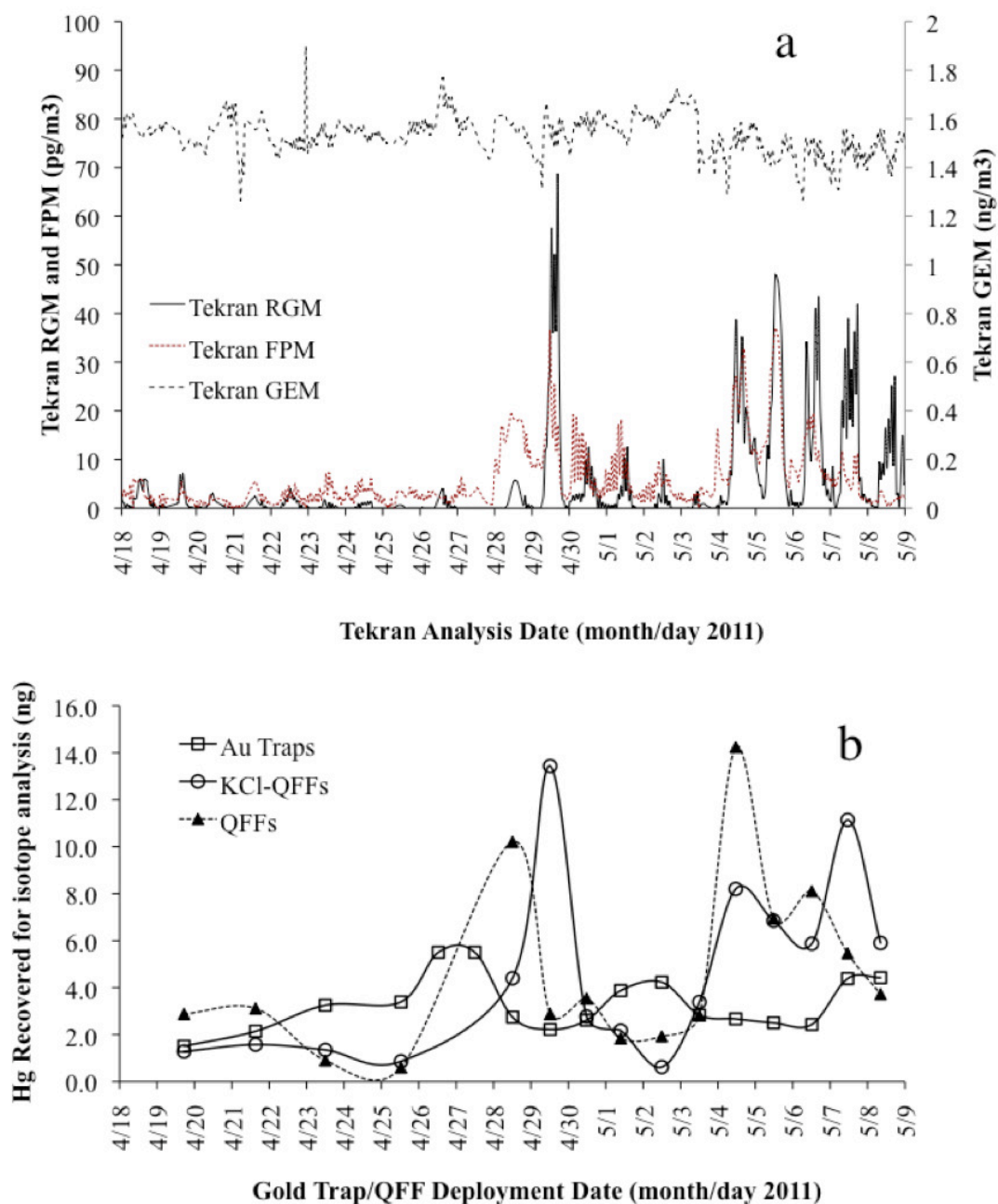


Figure 3.1: (a) Concentration of GEM, RGM, and FPM measured by dual Tekran[®] 2537A/1130/1135 automated Hg speciation analyzers (Winston Luke NOAA/OAR unpublished data) and (b) mass of Hg collected concurrently on gold traps, KCl treated quartz fiber filters, and untreated quartz fiber filters.

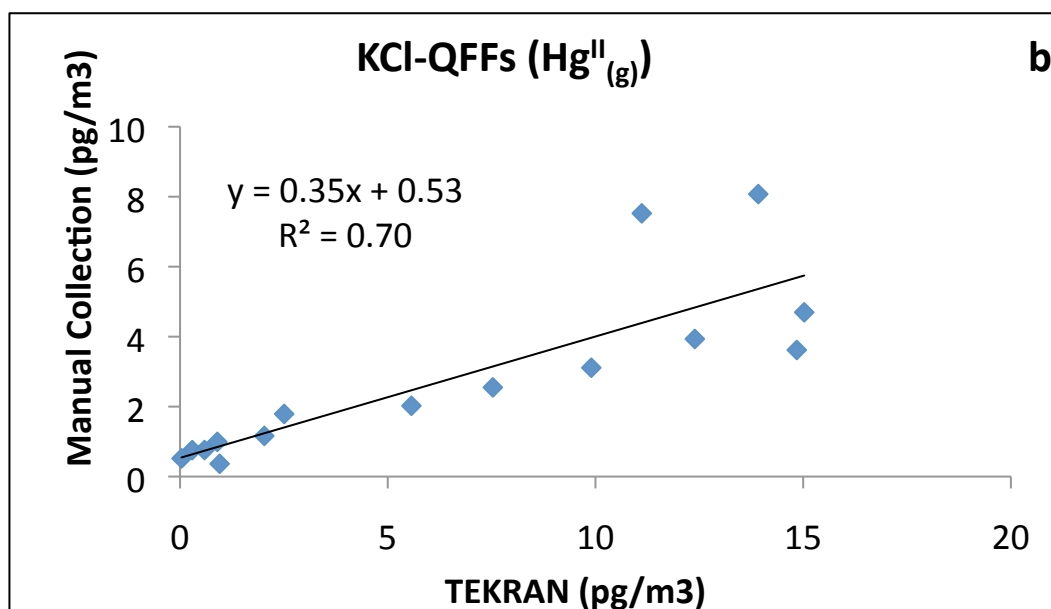
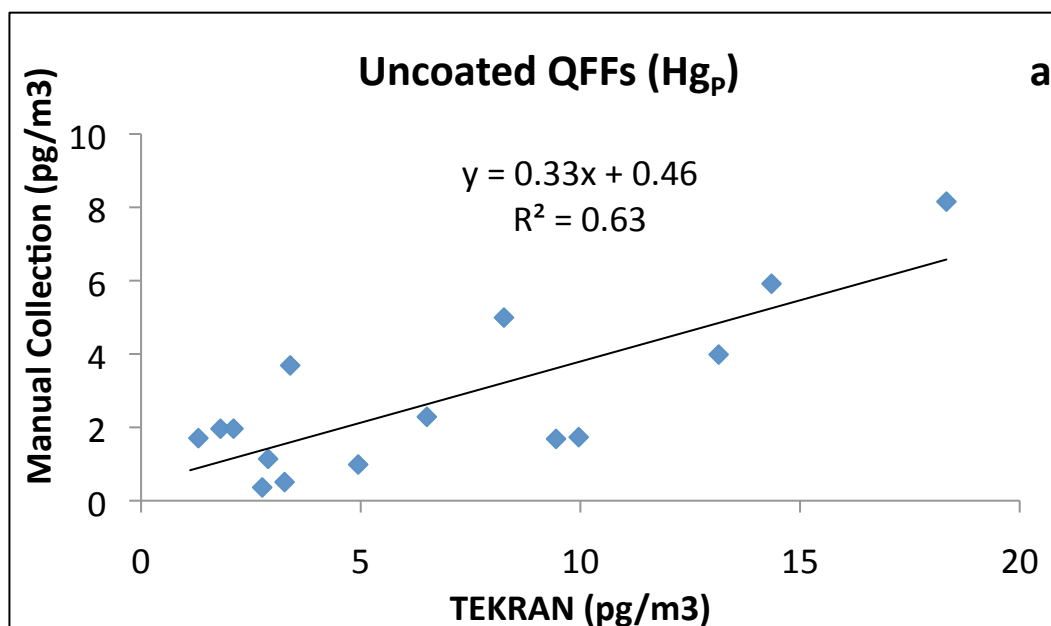


Figure 3.2: Comparison of average daily concentrations of Hg_p (A) and $\text{Hg}^{\text{II}}_{(g)}$ (B) as measured by the Tekran[®] 2537A/1130/1135 automated Hg speciation analyzers and the manual collection method employed for isotope analysis.

Table 3.1: Replicate analysis of sectioned untreated quartz fiber filters deployed at the OLF site for approximately 72 h. Concentrations were determined via CV-MC-ICPMS ^{202}Hg signals. Sample OLF 4.c suffered from a low carrier gas flow rate during the combustion process, which resulted in a decreased recovery.

Sample	Hg/sample ng	$\delta^{199}\text{Hg}$ ‰	$\delta^{200}\text{Hg}$ ‰	$\delta^{201}\text{Hg}$ ‰	$\delta^{202}\text{Hg}$ ‰	$\delta^{204}\text{Hg}$ ‰	$\Delta^{199}\text{Hg}$ ‰	$\Delta^{200}\text{Hg}$ ‰	$\Delta^{201}\text{Hg}$ ‰	$\Delta^{204}\text{Hg}$ ‰
OLF QFF-1										
a	5.2	0.03	-0.41	-0.46	-0.90	-1.74	0.26	0.05	0.22	-0.40
b	3.8	-0.06	-0.53	-0.65	-1.13	-1.38	0.23	0.03	0.20	0.30
c	4.5	0.02	-0.46	-0.59	-1.09	-1.43	0.30	0.09	0.23	0.20
	Average	0.00	-0.47	-0.57	-1.04	-1.52	0.26	0.06	0.21	0.04
	2SD	0.10	0.13	0.19	0.24	0.39	0.07	0.07	0.04	0.75
OLFQFF- 2										
a	6.7	-0.17	-0.38	-0.74	-1.05	-1.65	0.09	0.15	0.04	-0.09
b	8.4	-0.21	-0.48	-0.86	-1.14	-1.80	0.08	0.09	-0.01	-0.10
c	8.6	-0.05	-0.31	-0.72	-0.98	-1.51	0.20	0.18	0.02	-0.04
	Average	-0.14	-0.39	-0.77	-1.05	-1.65	0.12	0.14	0.02	-0.08
	2SD	0.17	0.17	0.15	0.15	0.29	0.13	0.09	0.05	0.06
OLF QFF-3										
a	10.2	0.19	-0.20	-0.31	-0.75	-1.28	0.38	0.18	0.26	-0.16
b	11.2	0.21	-0.16	-0.24	-0.70	-1.24	0.38	0.19	0.28	-0.20
c	8.0	0.16	-0.22	-0.36	-0.78	-1.35	0.36	0.18	0.23	-0.18
	Average	0.18	-0.19	-0.30	-0.74	-1.29	0.37	0.18	0.26	-0.18
	2SD	0.05	0.05	0.12	0.09	0.11	0.03	0.01	0.06	0.04
OLF QFF-4										
a	9.7	0.41	0.08	0.17	-0.23	-0.47	0.47	0.20	0.34	-0.12
b	9.2	0.44	0.12	0.30	-0.11	-0.45	0.46	0.18	0.38	-0.29
c	2.6	0.48	0.13	0.21	-0.07	-0.34	0.50	0.17	0.27	-0.23
	Average	0.44	0.11	0.23	-0.14	-0.42	0.48	0.18	0.33	-0.21
	2SD	0.07	0.06	0.13	0.17	0.14	0.04	0.03	0.12	0.17
OLF QFF-5										
a	4.9	0.18	-0.18	-0.23	-0.60	-1.00	0.33	0.12	0.22	-0.11
b	5.4	0.20	-0.08	-0.07	-0.53	-0.95	0.33	0.18	0.33	-0.16
c	4.7	0.21	-0.09	-0.12	-0.46	-0.84	0.33	0.14	0.22	-0.16
	Average	0.20	-0.12	-0.14	-0.53	-0.93	0.33	0.15	0.26	-0.14
	2SD	0.04	0.10	0.16	0.14	0.17	0.01	0.06	0.13	0.05
Average 2SD		0.08	0.10	0.15	0.16	0.22	0.06	0.05	0.08	0.22

Table 3.2: Isotopic composition of $\text{Hg}^0_{(\text{g})}$ standard trapped directly in KMnO_4 trapping solution and $\text{Hg}^0_{(\text{g})}$ standard initially trapped on a Au trap before being thermally released and then trapped in KMnO_4 trapping solution. Also included is the average UM-Almadén value obtained during analytical sessions from May 2011 to October 2011.

Sample	Hg/sample ng	$\delta^{199}\text{Hg}$ ‰	$\delta^{200}\text{Hg}$ ‰	$\delta^{201}\text{Hg}$ ‰	$\delta^{202}\text{Hg}$ ‰	$\delta^{204}\text{Hg}$ ‰	$\Delta^{199}\text{Hg}$ ‰	$\Delta^{200}\text{Hg}$ ‰	$\Delta^{201}\text{Hg}$ ‰	$\Delta^{204}\text{Hg}$ ‰
Elemental Hg vapor standard collected in KMnO_4 trapping solution										
a		-0.19	-0.63	-0.87	-1.34	-1.96	0.15	0.04	0.14	0.05
b		-0.10	-0.55	-0.83	-1.25	-1.80	0.21	0.07	0.11	0.06
c		-0.22	-0.70	-0.97	-1.42	-2.00	0.14	0.02	0.10	0.12
	Average	-0.17	-0.63	-0.89	-1.34	-1.92	0.16	0.04	0.12	0.08
	2SD	0.12	0.14	0.14	0.17	0.21	0.08	0.06	0.04	0.08
Gold traps loaded with elemental Hg vapor standard										
a		-0.21	-0.64	-0.86	-1.25	-1.93	0.11	-0.01	0.08	-0.06
b		-0.15	-0.66	-0.85	-1.28	-1.89	0.17	-0.02	0.11	0.02
c		-0.21	-0.68	-0.96	-1.38	-1.98	0.14	0.01	0.08	0.08
	Average	-0.19	-0.66	-0.89	-1.30	-1.93	0.14	0.00	0.09	0.01
	2SD	0.06	0.05	0.12	0.13	0.09	0.06	0.03	0.03	0.14
UM-Almadén Standard, n = 30										
	Average	-0.18	-0.32	-0.54	-0.66	-0.98	-0.01	0.01	-0.04	0.00
	2SD	0.08	0.07	0.09	0.09	0.16	0.07	0.06	0.07	0.11

Table 3.3: Isotopic composition of species-specific atmospheric Hg samples collected at Grand Bay, Mississippi (USA) during April-May, 2011. $\text{Hg}^0_{(\text{g})}$ was collected on gold traps, $\text{Hg}^{\text{II}}_{(\text{g})}$ was collected on KCl treated quartz fiber filters, and $\text{Hg}_{(\text{p})}$ was collected on untreated quartz fiber filters.

Site	Deployment Date	Recovery Date	Hg/sample ng	$\delta^{199}\text{Hg}$ ‰	$\delta^{200}\text{Hg}$ ‰	$\delta^{201}\text{Hg}$ ‰	$\delta^{202}\text{Hg}$ ‰	$\delta^{204}\text{Hg}$ ‰	$\Delta^{199}\text{Hg}$ ‰	$\Delta^{200}\text{Hg}$ ‰	$\Delta^{201}\text{Hg}$ ‰	$\Delta^{204}\text{Hg}$ ‰
<i>Gold Traps ($\text{Hg}^0_{(\text{g})}$)</i>												
GB	04/19/11	04/20/11	1.5									
GB	04/20/11	04/21/11										
GB	04/21/11	04/22/11	2.1									
GB	04/22/11	04/23/11										
GB	04/23/11	04/24/11	3.2									
GB	04/24/11	04/25/11										
GB	04/25/11	04/26/11	3.4	-0.81	-1.32	-1.94	-2.39	-3.52	-0.20	-0.12	-0.14	0.06
GB	04/26/11	04/28/11	11.0	-0.34	-0.23	-0.45	-0.33	-0.34	-0.26	-0.06	-0.20	0.14
GB	04/28/11	04/29/11	2.7	-0.47	-0.74	-1.03	-1.31	-1.91	-0.14	-0.08	-0.05	0.05
GB	04/29/11	04/30/11	2.2	-1.18	-2.11	-3.12	-3.88	-6.17	-0.21	-0.16	-0.20	-0.37
GB	04/30/11	05/01/11	2.6	-1.31	-1.97	-3.01	-3.58	-5.36	-0.41	-0.17	-0.32	-0.01
GB	05/01/11	05/02/11	3.9	-1.08	-1.75	-2.67	-3.22	-4.70	-0.27	-0.13	-0.25	0.11
GB	05/02/11	05/03/11	4.2	-1.01	-1.55	-2.40	-2.88	-4.23	-0.29	-0.10	-0.23	0.09
GB	05/03/11	05/04/11	2.8	-1.18	-1.82	-2.68	-3.24	-4.79	-0.37	-0.19	-0.25	0.05
GB	05/04/11	05/05/11	2.7	-1.11	-1.74	-2.75	-3.28	-5.04	-0.28	-0.09	-0.29	-0.14
GB	05/05/11	05/06/11	2.5	-0.96	-2.00	-2.80	-3.67	-5.44	-0.03	-0.16	-0.04	0.05
GB	05/06/11	05/07/11	2.4	-1.07	-1.83	-2.77	-3.45	-5.01	-0.20	-0.10	-0.18	0.15
GB	05/07/11	05/08/11	4.4	-0.92	-1.41	-2.20	-2.63	-3.89	-0.26	-0.09	-0.23	0.04
GB	05/08/11	05/09/11	4.4	-0.60	-0.71	-1.23	-1.27	-1.81	-0.28	-0.07	-0.27	0.09
<i>KCl-QFFs ($\text{Hg}^{\text{II}}_{(\text{g})}$)</i>												
GB	04/19/11	04/20/11	1.3									
GB	04/20/11	04/21/11										
GB	04/21/11	04/22/11	1.6									
GB	04/22/11	04/23/11										
GB	04/23/11	04/24/11	1.3									
GB	04/24/11	04/25/11										
GB	04/25/11	04/26/11	0.9									
GB	04/26/11	04/28/11										
GB	04/28/11	04/29/11	4.4	0.28	0.98	1.03	1.41	1.77	-0.07	0.28	-0.03	-0.32
GB	04/29/11	04/30/11	13.4	0.30	0.94	1.03	1.45	1.85	-0.07	0.21	-0.06	-0.32
GB	04/30/11	05/01/11	2.8	0.23	0.73	0.92	1.29	1.64	-0.10	0.08	-0.04	-0.28
GB	05/01/11	05/02/11	2.2	0.15	0.88	1.11	1.57	2.65	-0.24	0.09	-0.07	0.31
GB	05/02/11	05/03/11	0.6									
GB	05/03/11	05/04/11	3.4	0.16	0.41	0.37	0.51	0.63	0.03	0.16	-0.02	-0.13
GB	05/04/11	05/05/11	8.2	0.31	1.03	1.06	1.58	1.94	-0.09	0.24	-0.13	-0.41
GB	05/05/11	05/06/11	6.9	0.10	0.85	0.64	1.19	1.62	-0.20	0.26	-0.25	-0.15
GB	05/06/11	05/07/11	5.9	0.05	0.83	0.70	1.23	1.57	-0.26	0.21	-0.23	-0.27
GB	05/07/11	05/08/11	11.1	0.38	0.58	0.78	0.79	1.00	0.18	0.18	0.19	-0.18
GB	05/08/11	05/09/11	5.9	0.13	0.92	1.00	1.61	2.31	-0.28	0.11	-0.22	-0.09

Table 3.3 *continued*.

Site	Deployment Date	Recovery Date	Hg/sample ng	$\delta^{199}\text{Hg}$ ‰	$\delta^{200}\text{Hg}$ ‰	$\delta^{201}\text{Hg}$ ‰	$\delta^{202}\text{Hg}$ ‰	$\delta^{204}\text{Hg}$ ‰	$\Delta^{199}\text{Hg}$ ‰	$\Delta^{200}\text{Hg}$ ‰	$\Delta^{201}\text{Hg}$ ‰	$\Delta^{204}\text{Hg}$ ‰
<i>Untreated QFFs ($\text{Hg}_{(p)}$)</i>												
GB	04/19/11	04/20/11	2.9									
GB	04/20/11	04/21/11										
GB	04/21/11	04/22/11	3.1									
GB	04/22/11	04/23/11										
GB	04/23/11	04/24/11	0.9									
GB	04/24/11	04/25/11										
GB	04/25/11	04/26/11	0.6									
GB	04/26/11	04/28/11										
GB	04/28/11	04/29/11	10.2	0.33	-0.21	-0.21	-0.92	-1.76	0.56	0.25	0.48	-0.38
GB	04/29/11	04/30/11	2.9	-0.01	-0.72	-0.84	-1.61	-3.24	0.39	0.09	0.37	-0.84
GB	04/30/11	05/01/11	3.5	0.86	0.06	0.72	-0.12	-0.55	0.89	0.12	0.81	-0.37
GB	05/01/11	05/02/11	1.8	0.51	-0.36	-0.07	-0.98	-2.04	0.75	0.13	0.66	-0.58
GB	05/02/11	05/03/11	1.9									
GB	05/03/11	05/04/11	2.8	0.56	-0.48	-0.22	-1.19	-1.92	0.86	0.12	0.68	-0.14
GB	05/04/11	05/05/11	14.2	1.07	-0.14	0.54	-0.79	-1.49	1.27	0.26	1.13	-0.31
GB	05/05/11	05/06/11	6.9	0.50	-0.30	-0.02	-0.85	-1.37	0.71	0.13	0.62	-0.09
GB	05/06/11	05/07/11	8.1	1.09	0.05	0.80	-0.28	-0.58	1.16	0.18	1.01	-0.17
GB	05/07/11	05/08/11	5.5	1.00	-0.67	0.12	-1.44	-2.40	1.36	0.06	1.20	-0.25
GB	05/08/11	05/09/11	3.7	0.24	-0.14	-0.06	-0.49	-0.88	0.36	0.10	0.30	-0.15

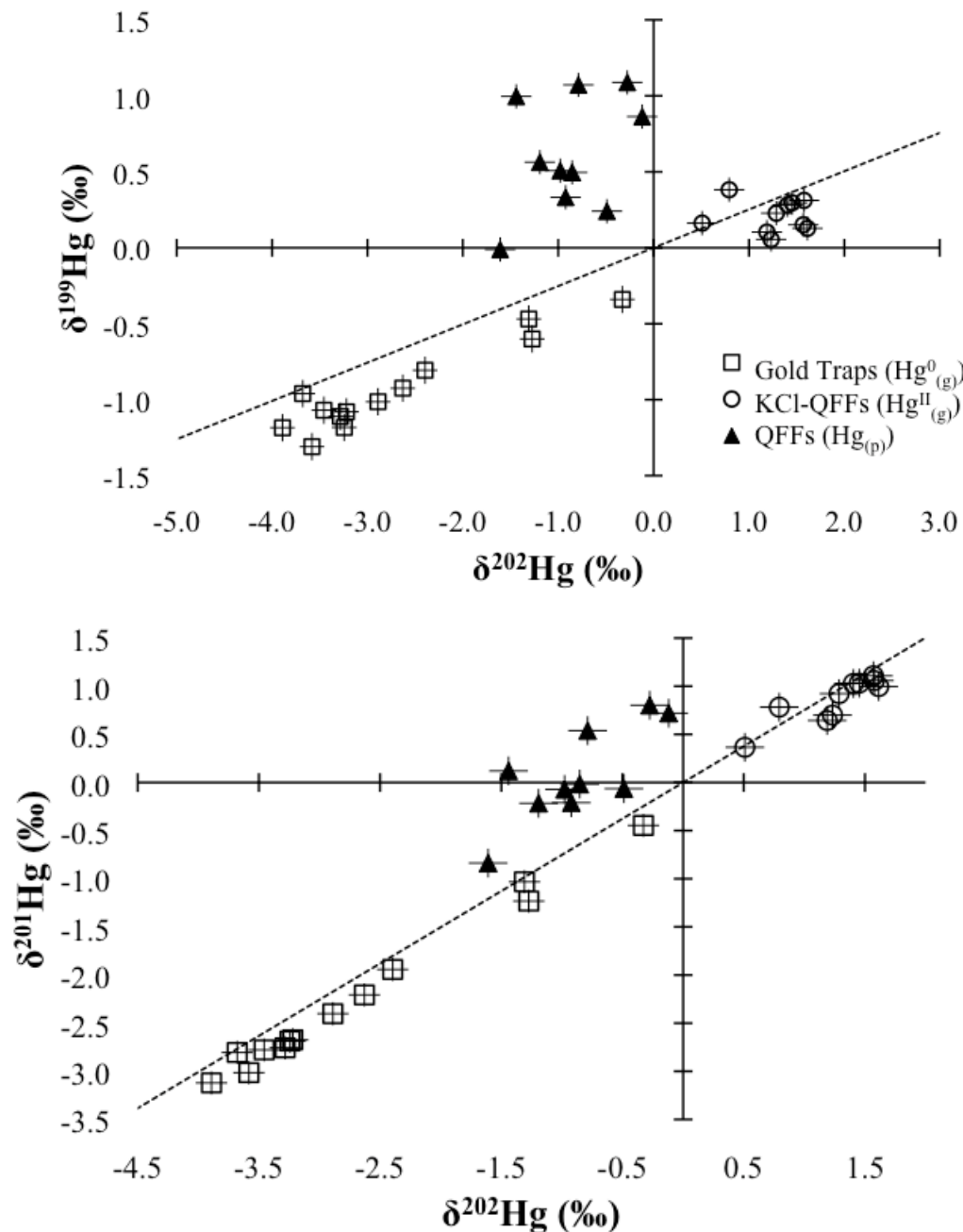


Figure 3.3: ^{199}Hg and ^{201}Hg three isotope diagrams for species-specific atmospheric Hg samples collected at Grand Bay, Mississippi (USA) during April-May, 2011. Isotopic compositions of $\text{Hg}^0_{(\text{g})}$ (open squares), $\text{Hg}_{(\text{p})}$ (black triangles), and $\text{Hg}^{\text{II}}_{(\text{g})}$ (open circles) are plotted. Dashed lines represent theoretical mass dependent fractionation (MDF). Points that do not fall on the MDF line indicate anomalous mass-independent fractionation (MIF). Uncertainties are determined by the reproducibility of the UM-Almadén standard and procedural replicates and standards (see text).

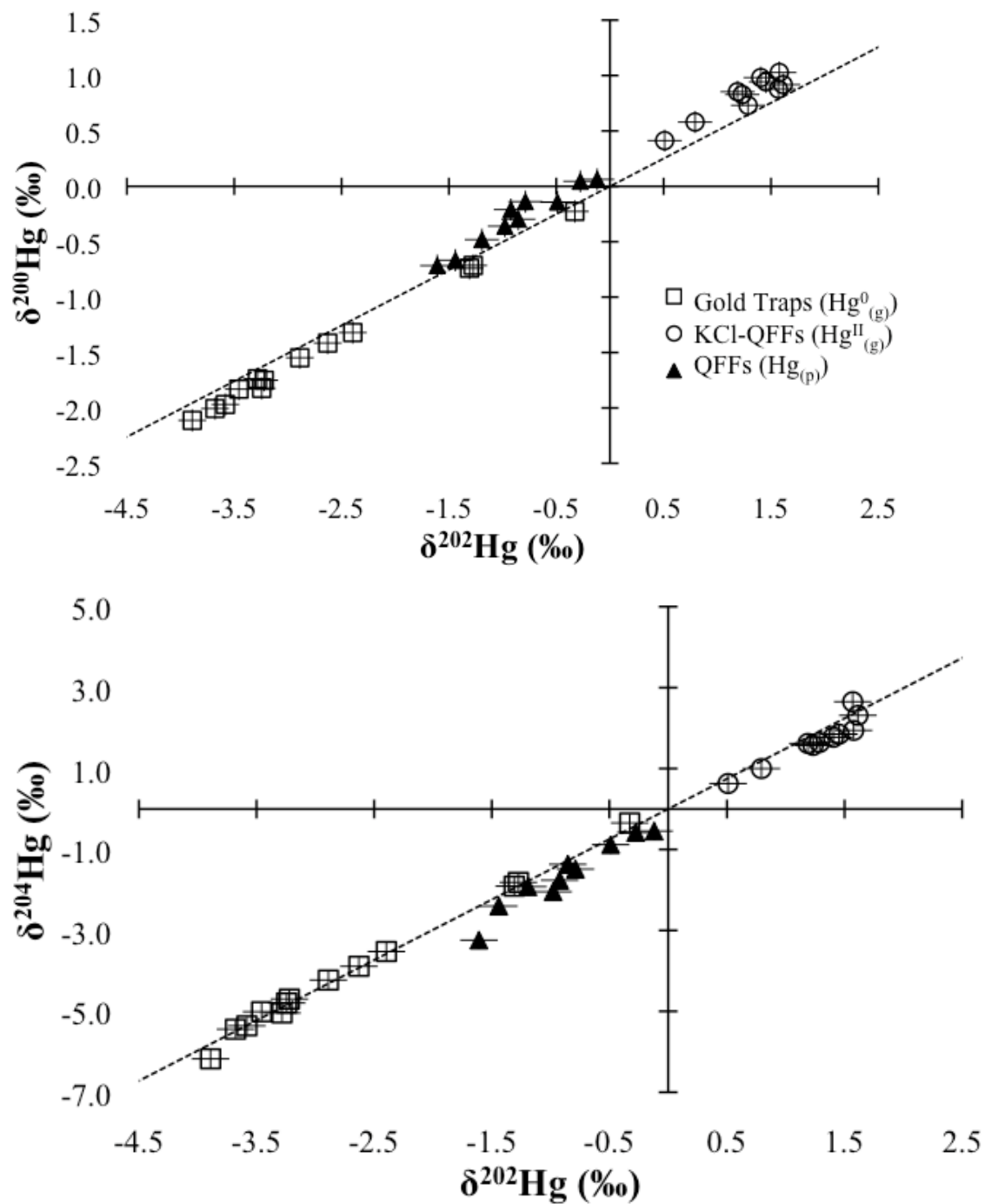


Figure 3.4: ^{200}Hg and ^{204}Hg three isotope diagrams for species-specific atmospheric Hg samples collected at Grand Bay, Mississippi (USA) during April-May, 2011. Isotopic compositions of $\text{Hg}^0_{(\text{g})}$ (open squares), $\text{Hg}_{(\text{p})}$ (black triangles), and $\text{Hg}^{\text{II}}_{(\text{g})}$ (open circles) are plotted. Dashed lines represent theoretical mass dependent fractionation (MDF). Points that do not fall on the MDF line indicate anomalous mass-independent fractionation (MIF). Uncertainties are determined by the reproducibility of the UM-Almadén standard and procedural replicates and standards (see text).

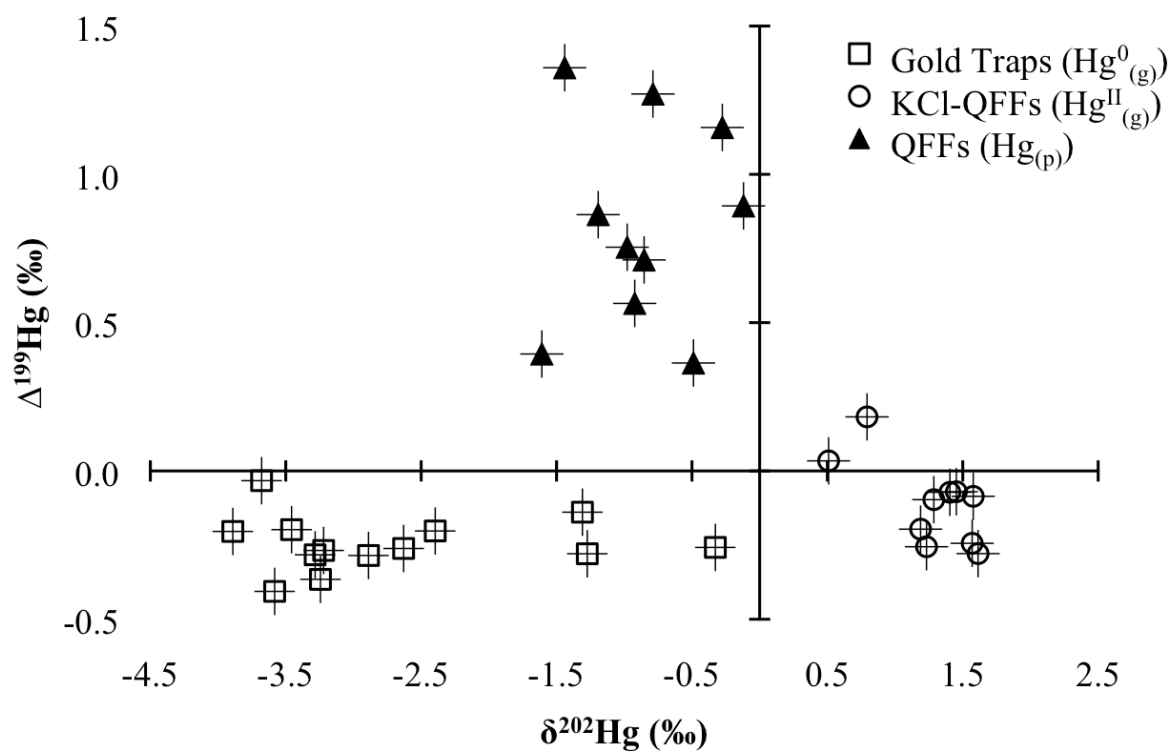


Figure 3.5: $\Delta^{199}\text{Hg}$ (‰) versus $\delta^{202}\text{Hg}$ (‰) for atmospheric Hg samples collected at Grand Bay, Mississippi (USA) during April-May, 2011. Data points represent $\text{Hg}^0_{(\text{g})}$ (open squares), $\text{Hg}_{(\text{p})}$ (black triangles), and $\text{Hg}^{\text{II}}_{(\text{g})}$ (open circles). Uncertainties are determined by the reproducibility of the UM-Almadén standard and procedural replicates and standards (see text).

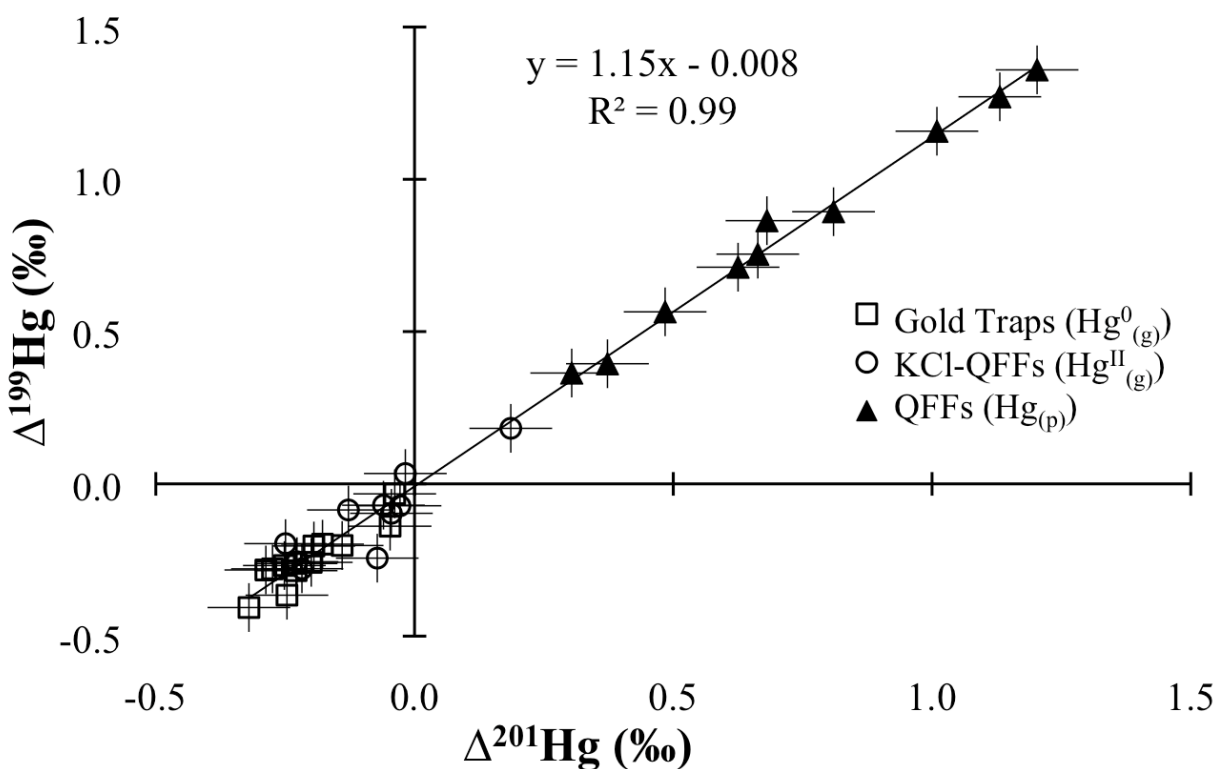


Figure 3.6: $\Delta^{199}\text{Hg}$ (‰) versus $\Delta^{201}\text{Hg}$ (‰) for atmospheric Hg samples collected at Grand Bay, Mississippi (USA) during April-May, 2011. Data points represent $\text{Hg}^0_{(\text{g})}$ (open squares), $\text{Hg}_{(\text{p})}$ (black triangles), and $\text{Hg}^{\text{II}}_{(\text{g})}$ (open circles). Uncertainties are determined by the reproducibility of the UM-Almadén standard and procedural replicates and standards (see text).

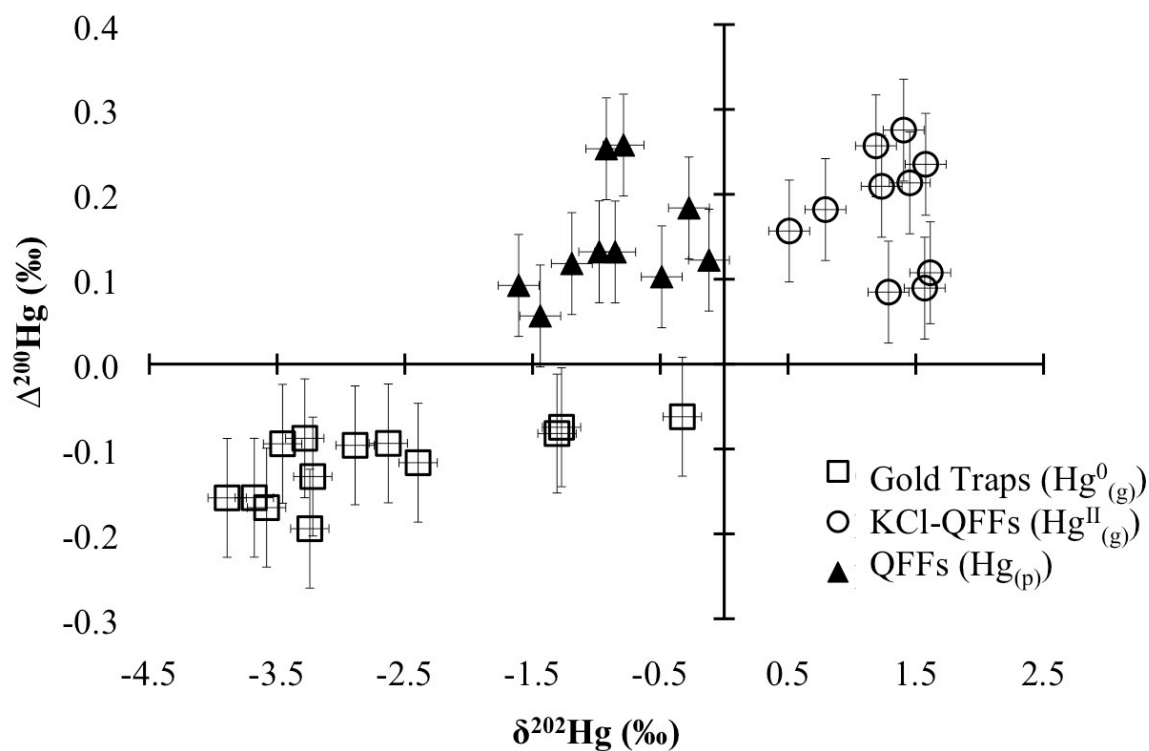


Figure 3.7: $\Delta^{200}\text{Hg}$ (‰) versus $\delta^{202}\text{Hg}$ (‰) for atmospheric Hg samples collected at Grand Bay, Mississippi (USA) during April-May, 2011. Data points represent $\text{Hg}^0_{(\text{g})}$ (open squares), $\text{Hg}_{(\text{p})}$ (black triangles), and $\text{Hg}^{\text{II}}_{(\text{g})}$ (open circles). Uncertainties are determined by the reproducibility of the UM-Almadén standard and procedural replicates and standards (see text).

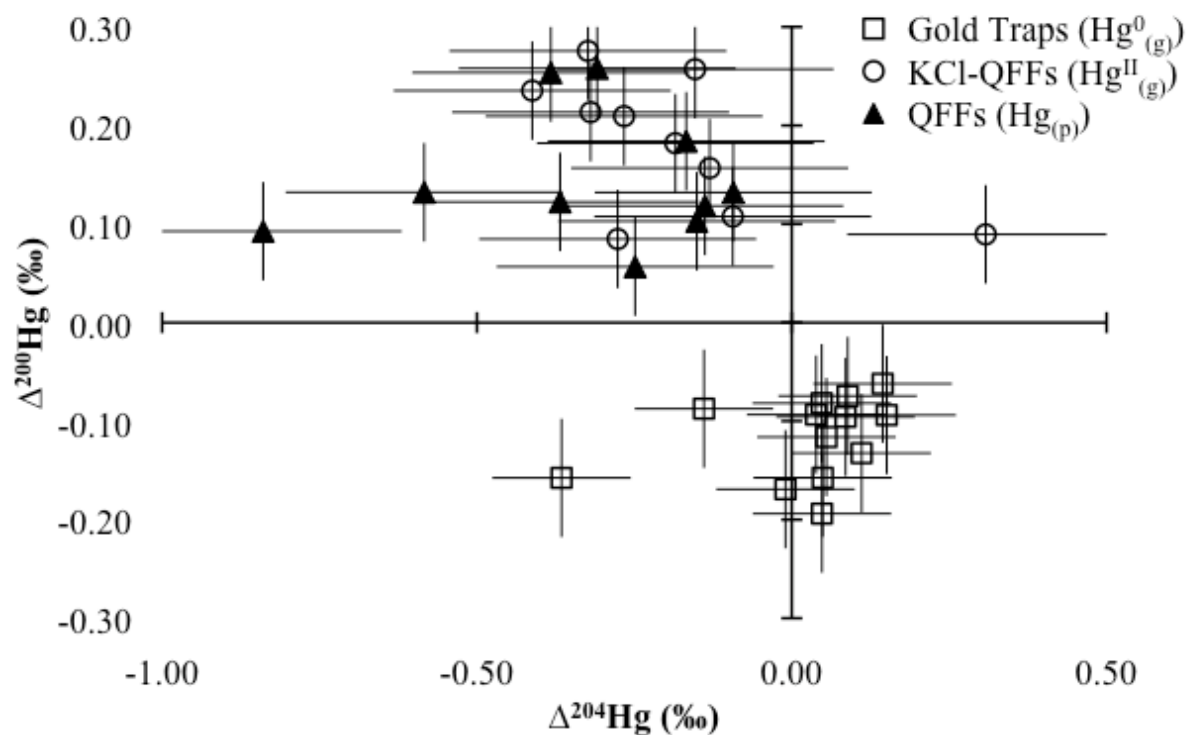


Figure 3.8: $\Delta^{200}\text{Hg}$ (‰) versus $\Delta^{204}\text{Hg}$ (‰) for atmospheric Hg samples collected at Grand Bay, Mississippi (USA) during April-May, 2011. Data points represent $\text{Hg}^0_{(\text{g})}$ (open squares), $\text{Hg}_{(\text{p})}$ (black triangles), and $\text{Hg}^{\text{II}}_{(\text{g})}$ (open circles). Uncertainties are determined by the reproducibility of the UM-Almadén standard and procedural replicates and standards (see text).

CHAPTER FOUR

DISCUSSION

4.1 Mass dependent fractionation of $\text{Hg}^0_{(\text{g})}$

Although Hg stable isotope geochemistry has been established as a powerful tool for studying the complex biogeochemical cycle of Hg, few studies have focused on direct isotopic composition measurements of atmospheric Hg species (Zambardi et al., 2009; Sherman et al., 2010, 2012; Gratz et al., 2010). Rather, the isotopic composition of atmospheric Hg has been investigated indirectly by measuring the isotopic composition of Hg in reservoirs that are considered tracers of atmospheric Hg deposition such as lichens, moss, peat, coal, soils, and sediments (Biswas et al., 2008; Ghosh et al., 2008; Carignan et al., 2009; Estrade et al., 2010; Sonke et al., 2010). This is primarily due to the analytical challenge of measuring the isotopic compositions of low-level atmospheric Hg species. The objective of this study was to directly analyze the isotopic composition of the individual atmospheric Hg species.

Mass dependent fractionation will be discussed in terms of $\delta^{202}\text{Hg}$. For $\text{Hg}^0_{(\text{g})}$, the $\delta^{202}\text{Hg}$ values reported here are more negative than previous reports (Zambardi et al., 2009; Sherman et al., 2010; Gratz et al., 2010). However, the sampling locations were drastically different for each study. Zambardi et al. (2009) collected $\text{Hg}^0_{(\text{g})}$ in a fumarole plume. Sherman et al. (2010) collected $\text{Hg}^0_{(\text{g})}$ in the Arctic and Gratz et al. (2010) collected $\text{Hg}^0_{(\text{g})}$ in the Great Lakes region of the United States. In our study, air masses were sampled at GB in a semi-rural coastal environment at ~2 m above sea level. It could be expected that air masses originating offshore may contain significant Hg derived from long-range transport or emissions from surface waters (Strode et al., 2007). However, local anthropogenic sources may influence air masses that appear to originate offshore due to alternating wind directions between sea breeze and land breeze. Therefore, potential sources of $\text{Hg}^0_{(\text{g})}$ include long-range transport, Hg that has been emitted from Gulf of Mexico surface waters, local/regional anthropogenic emission sources, and possibly minor amounts of $\text{Hg}^0_{(\text{g})}$ emitted from local soils and vegetation. Although the isotopic compositions of potential sources of long-range transport and local/regional anthropogenic sources are unknown, the photoreduction of dissolved Hg^{II} ($\text{Hg}^{\text{II}}_{(\text{aq})}$) and subsequent volatilization of the product, $\text{Hg}^0_{(\text{g})}$, has been shown to follow mass dependent fractionation,

which predicts enrichment of light isotopes in product $\text{Hg}^0_{(g)}$ (Bergquist and Blum, 2007; Zheng et al., 2007; Zheng and Hintelmann, 2009). Accordingly, low $\delta^{202}\text{Hg}$ values for $\text{Hg}^0_{(g)}$ are expected in marine air masses that contain significant $\text{Hg}^0_{(g)}$ produced by volatilization from surface waters, but have not experienced significant mixing with air mass containing $\text{Hg}^0_{(g)}$ with high $\delta^{202}\text{Hg}$ values. Therefore, the low $\text{Hg}^0_{(g)}$ $\delta^{202}\text{Hg}$ values reported here potentially signify that the evasion flux of Hg from surface water contributes significantly to atmospheric $\text{Hg}^0_{(g)}$ along the northern coast of the Gulf of Mexico.

Alternatively, $\text{Hg}^0_{(g)}$ with low $\delta^{202}\text{Hg}$ values could reflect fractionation induced by atmospheric processes, such as oxidation and/or deposition, during long range transport. Deposition may be especially important due to the sampling location being near ground level and in the vicinity of vegetated surfaces. Deposition of Hg is driven by $\text{Hg}_{(p)}$ and $\text{Hg}^{\text{II}}_{(g)}$ however, and therefore $\text{Hg}^0_{(g)}$ should be least affected by local depositional processes. The $\delta^{202}\text{Hg}$ values of $\text{Hg}^0_{(g)}$ could be driven to lower values during long range transport by continual oxidation and subsequent deposition of isotopically heavy divalent Hg species. Additionally, known local/regional anthropogenic emission sources possibly contributing to the atmospheric Hg at GB include coal fired power plants. Biswas et al. (2008) measured $\delta^{202}\text{Hg}$ values from -3‰ to -0.5‰ in a variety of United States coals. However, it is not known if, or to what extent, Hg isotopes are fractionated during combustion and emission. The use of scrubbers to remove Hg from emissions most likely induces significant fractionation of the fraction of Hg that is emitted. The range in $\delta^{202}\text{Hg}$ measured in atmospheric $\text{Hg}^0_{(g)}$ at GB likely represent mixing of multiple natural and anthropogenic sources.

4.2 Mass dependent fractionation of $\text{Hg}_{(p)}$ and $\text{Hg}^{\text{II}}_{(g)}$

The oxidation of $\text{Hg}^0_{(g)}$ to divalent Hg species in the marine environment is driven by the presence of halogen atoms, especially atomic bromine (Mason and Sheu, 2002; Holmes et al., 2009; Obrist et al., 2010). Atomic Cl and Br are generated by the photolysis of weakly bound nighttime reservoirs during sunrise, which subsequently drives the observed diurnal variation in $\text{Hg}^{\text{II}}_{(g)}$ (Holmes et al., 2009). The $\text{Hg}^{\text{II}}_{(g)}$ $\delta^{202}\text{Hg}$ values suggests that during oxidation, equilibrium isotope fractionation dominates over potentially present kinetic isotope fractionation, resulting in the observed enrichment of heavier isotopes in $\text{Hg}^{\text{II}}_{(g)}$ relative to $\text{Hg}^0_{(g)}$. The mass dependent fractionation factor between $\text{Hg}^{\text{II}}_{(g)}$ and $\text{Hg}^0_{(g)}$ was calculated using Eq. (6):

$$\alpha_{oxidized-elemental}^{202/198} = \frac{\left(\frac{^{202}\text{Hg}}{^{198}\text{Hg}} \right)_{oxidized}}{\left(\frac{^{202}\text{Hg}}{^{198}\text{Hg}} \right)_{reduced}} = \frac{(\delta^{202}\text{Hg}_{gas}^{II}/1000 + 1)}{(\delta^{202}\text{Hg}_{gas}^0/1000 + 1)} \quad (6)$$

The $\delta^{202}\text{Hg}$ values for concurrently collected $\text{Hg}_{(g)}^{II}$ and $\text{Hg}_{(g)}^0$ were used to calculate an average fractionation factor, $\alpha_{\text{Hg}_{(g)}^{II}-\text{Hg}_{(g)}^0}^{202/198} = 1.00423 \pm 0.00095$ (1SD, n=10). Using first-principles vibrational frequency and electronic structure calculations, Schauble (2007) predicted theoretical equilibrium isotope fractionation factors between $\text{Hg}_{(g)}^0$ and $\text{Hg}_{(g)}^{II}$ species such as HgCl_2 and HgBr_2 . At 0 °C the theoretical total fractionation factors $\alpha_{\text{HgCl}_2-\text{Hg}_{(g)}^0}^{202/198}$ and $\alpha_{\text{HgBr}_2-\text{Hg}_{(g)}^0}^{202/198}$ are 1.00247 and 1.00229, respectively, both of which differ significantly from our measured fractionation factor.

The large discrepancy between the measured $\alpha_{\text{Hg}_{(g)}^{II}-\text{Hg}_{(g)}^0}^{202/198}$ and theoretical $\alpha_{\text{HgCl}_2-\text{Hg}_{(g)}^0}^{202/198}$ and $\alpha_{\text{HgBr}_2-\text{Hg}_{(g)}^0}^{202/198}$ may be explained by additional isotope fractionation during the conversion of $\text{Hg}_{(g)}^{II}$ to $\text{Hg}_{(p)}$. Due to the short atmospheric lifetime of aerosols (hours to weeks), the uptake of $\text{Hg}_{(g)}^{II}$ into aerosols (i.e. $\text{Hg}_{(p)}$) is limited by diffusion, which inhibits equilibrium between $\text{Hg}_{(g)}^{II}$ and $\text{Hg}_{(p)}$. Diffusion inherently induces kinetic isotope fractionation because lighter isotopes diffuse faster than heavier isotopes. Since $\text{Hg}_{(g)}^{II}$ is diffusing in to the aerosol, the remaining reservoir of $\text{Hg}_{(g)}^{II}$ should become enriched in heavier Hg isotopes while $\text{Hg}_{(p)}$ should become enriched in lighter Hg isotopes. This is supported by the observations that the $\text{Hg}_{(p)}$ $\delta^{202}\text{Hg}$ values are lighter than concurrently collected $\text{Hg}_{(g)}^{II}$ $\delta^{202}\text{Hg}$ values and $\alpha_{\text{Hg}_{(p)}-\text{Hg}_{(g)}^{II}}^{202/198} = 0.99668 \pm 0.00097$ (1SD, n=5). Therefore, the $\text{Hg}_{(g)}^{II}$ $\delta^{202}\text{Hg}$ appears to be the result of MDF induced by two or more processes (i.e. oxidation and diffusion), which may account for the discrepancy between $\alpha_{\text{Hg}_{(g)}^{II}-\text{Hg}_{(g)}^0}^{202/198}$ measured here and theoretical $\alpha_{\text{HgCl}_2-\text{Hg}_{(g)}^0}^{202/198}$ and $\alpha_{\text{HgBr}_2-\text{Hg}_{(g)}^0}^{202/198}$ predicted by Schauble (2007).

4.3 Mass independent fractionation (MIF)

4.3.1 MIF mechanisms

MIF of ^{199}Hg and ^{201}Hg has been explained by two mechanisms: the magnetic isotope effect (MIE) and the nuclear volume effect (NVE). The NVE arises due to the non-linear increase between the Hg isotope number and the mean square nuclear charge radius, $\langle r^2 \rangle$. In particular, ^{199}Hg and ^{201}Hg are characterized by nuclear volume/shape distortions that give rise to smaller than expected $\langle r^2 \rangle$ (Schauble, 2007). NVE has been documented during elemental Hg^0 liquid-vapor equilibrium (Estrade et al. 2009, Ghosh et al., 2012), abiotic non-photochemical $\text{Hg}^{\text{II}}_{(\text{aq})}$ reduction (Zheng and Hintelmann, 2009, 2010b), and equilibrium $\text{Hg}^{\text{II}}_{(\text{aq})}$ -thiol complexation (Wiederhold et al, 2010).

The MIE occurs during photochemical reactions in which long-lived radical pairs are formed. Odd isotopes have a nuclear spin and associated nuclear magnetic moment that can interact with magnetic moments of electrons (i.e. nuclear-electronic hyperfine coupling) and change a reaction from the spin-forbidden to a spin-allowed state or from the spin-allowed to spin-forbidden state. This effect results in different reaction rates between even and odd isotopes of Hg during reactions involving long-lived radical pairs (Buchachenko, 2004; Zheng and Hintelmann, 2009, 2010a; Epov, 2011). Thus, isotope fractionation during radical reactions is dependent on a parameter other than mass.

Theory and observations suggest that NVE and MIE induce significantly different relationships between $\Delta^{199}\text{Hg}$ and $\Delta^{201}\text{Hg}$. All available theoretical and experimental evidence for NVE suggest a slope > 1.5 when $\Delta^{199}\text{Hg}$ is graphed against $\Delta^{201}\text{Hg}$. Experimental evidence of MIE results in a $\Delta^{199}\text{Hg}/\Delta^{201}\text{Hg}$ slope in the range of 1.00-1.36 (Bergquist and Blum, 2007; Zheng and Hintelmann, 2009, 2010a). In this study, all samples collected yielded a slope of $\Delta^{199}\text{Hg}/\Delta^{201}\text{Hg} = 1.15 \pm 0.02$ ($r^2 = 0.99$), indicating that the MIF signature in atmospheric Hg is likely to have been produced by the MIE (Fig. 3.6).

4.3.2 MIF in atmospheric Hg

Bergquist and Blum (2007) observed enrichments of ^{199}Hg and ^{201}Hg (i.e. positive MIF) in residual $\text{Hg}^{\text{II}}_{(\text{aq})}$ and methylmercury during laboratory experiments on $\text{Hg}^{\text{II}}_{(\text{aq})}$ photoreduction and methylmercury photodegradation in simulated natural waters. Zheng and Hintelmann (2009) collected the evading $\text{Hg}^0_{(\text{g})}$, during such experiments, and showed it to be depleted in the odd

isotopes relative to the residual $\text{Hg}^{\text{II}}_{(\text{aq})}$ (i.e. negative MIF). Furthermore, Hg in fish, which is dominantly methylmercury, was shown to carry significant positive MIF signatures (Bergquist and Blum, 2007; Das et al., 2009). Thus, it was predicted that atmospheric and aquatic reservoirs of Hg might contain complimentary MIF signatures (Bergquist and Blum, 2007; Carignan et al., 2009). However, direct measurements of atmospheric $\text{Hg}^0_{(\text{g})}$ by Gratz et al. (2010) and Sherman et al. (2010) showed minor MIF indicated by the range of $\Delta^{199}\text{Hg}$ from -0.22‰ to 0.06‰. Also, Hg^{II} in precipitation has significant positive $\Delta^{199}\text{Hg}$ ranging from +0.10‰ to +0.61‰ (Gratz et al., 2010). These observations question the importance of aquatic photoreduction as a source of MIF in atmospheric Hg (Gratz et al., 2010; Sonke, 2011). Furthermore, the possibility of biochemically induced MIF casts some doubt on the reliability of using bioaccumulators to approximate the isotopic composition of atmospheric Hg (Jackson et al., 2008; Das et al., 2009).

In this study, the isotopic compositions of atmospheric Hg species ($\text{Hg}^0_{(\text{g})}$, $\text{Hg}^{\text{II}}_{(\text{g})}$, and $\text{Hg}_{(\text{p})}$) were measured directly. $\text{Hg}^0_{(\text{g})}$ displayed negative values of $\Delta^{199}\text{Hg}$ (average = -0.25‰ \pm 0.09‰, 1SD, n = 13) and $\Delta^{201}\text{Hg}$ (average = -0.20‰ \pm 0.09‰, 1SD, n = 13). $\text{Hg}^0_{(\text{g})}$ with negative MIF is expected to be associated with photoreduction of $\text{Hg}^{\text{II}}_{(\text{aq})}$ (Bergquist and Blum, 2007; Zheng and Hintelmann, 2009). $\text{Hg}^0_{(\text{g})}$ with low $\delta^{202}\text{Hg}$ values and negative MIF in $\text{Hg}^0_{(\text{g})}$ also suggest that evasion of Hg from surface waters could be a significant source of atmospheric Hg along the northern coast of the Gulf of Mexico. Again however, a variety of U.S. coal deposits display similar MIF with $\Delta^{199}\text{Hg}$ and $\Delta^{201}\text{Hg}$ values ranging from -0.30‰ to +0.10‰ (Biswas et al. 2008; Lefticariu et al., 2011). $\text{Hg}^{\text{II}}_{(\text{g})}$ showed variable MIF with average $\Delta^{199}\text{Hg}$ and $\Delta^{201}\text{Hg}$ values ranging from -0.28‰ to +0.18‰ (average = -0.11‰ \pm 0.14‰; 1SD, n = 10) and -0.25‰ to +0.19‰ (average = -0.09‰ \pm 0.13; 1SD, n = 10), respectively. The small difference between MIF measured in $\text{Hg}^0_{(\text{g})}$ and $\text{Hg}^{\text{II}}_{(\text{g})}$ may indicate that atmospheric oxidation reactions do not induce significant MIF of Hg isotopes. Since oxidation by ozone or halogen radicals is not a direct photochemical process long-lived radical pairs are not produced and therefore no MIF from MIE is expected (Buchachenko, 2001; Zheng and Hintelmann, 2009, 2010a; Gratz et al., 2010).

The most significant MIF was measured in $\text{Hg}_{(\text{p})}$. Values of $\Delta^{199}\text{Hg}$ and $\Delta^{201}\text{Hg}$ range from +0.36‰ to +1.36‰ (average = 0.83 \pm 0.35; 1SD, n = 10) and +0.30‰ to +1.20‰ (average = 0.73 \pm 0.31; 1SD, n=10), respectively. Gratz et al. (2010) suggested that photoreduction of

Hg^{II} in cloud droplets containing organic matter may produce MIF similar to that observed in controlled photoreduction experiments and that cloud droplets would preferentially retain odd isotopes thereby becoming increasingly positive with respect to $\Delta^{199}\text{Hg}$ and $\Delta^{201}\text{Hg}$. This prediction was invoked to explain positive $\Delta^{199}\text{Hg}$ and $\Delta^{201}\text{Hg}$ measured in precipitation (Gratz et al., 2010). Significant positive Hg_(p) $\Delta^{199}\text{Hg}$ and $\Delta^{201}\text{Hg}$ measured in this study supports this hypothesis.

4.3.3 Modeling in-aerosol photoreduction

Sonke (2011) constructed a global Hg MIF box-model to simulate observed MIF signatures in environmental reservoirs. Total fractionation factors $\alpha_{TOT(0-II)}^{xxx/198}$ are the product of mass dependent and mass independent fractionation such that $\alpha_{TOT}^{xxx/198} = \alpha_{MDF}^{xxx/198} \times \alpha_{MIF}^{xxx/198}$. Sonke (2011) obtained optimum model results with in-aerosol MIF of magnitude $\alpha_{aerosol-MIF(0-II)}^{199/198} = 0.9993$, which suggest the accumulation of significantly positive $\Delta^{199}\text{Hg}$ in Hg_(p) resulting directly from in-aerosol photoreduction. The extent of in-aerosol photoreduction based on MIF can be modeled using a modified Rayleigh equation (Sonke, 2011):

$$10^3 \times \ln \frac{(10^{-3} \times \Delta^{199}\text{Hg}_{t=0}^{II} + 1)}{(10^{-3} \times \Delta^{199}\text{Hg}_{t=t}^{II} + 1)} = \epsilon_{aerosol-MIF(0-II)}^{199/198} \times \ln f \quad (6)$$

where $\Delta^{199}\text{Hg}_{t=0}^{II}$ and $\Delta^{199}\text{Hg}_{t=t}^{II}$ are the measured $\text{Hg}_{(p)}^{II}$ $\Delta^{199}\text{Hg}$ at time $t = 0$ and time ' t ', and f is the fraction of $\text{Hg}_{(p)}^{II}$ remaining at time ' t '. $\epsilon_{aerosol-MIF(0-II)}^{199/198}$ is the 'permil fractionation factor': $\epsilon_{aerosol-MIF(0-II)}^{199/198} = 10^3 \times (\alpha_{aerosol-MIF(0-II)}^{199/198} - 1)$. Therefore, $\epsilon_{aerosol-MIF(0-II)}^{199/198} = -0.7\text{‰}$ under optimal model conditions and indicates that during photoreduction of Hg_(p)^{II}, the instantaneous production of Hg_(g)⁰ has a $\Delta^{199}\text{Hg}$ anomaly of -0.7‰ (Sonke, 2011). Under the assumptions that no MIF takes place during $\text{Hg}_{(g)}^{II} \rightarrow \text{Hg}_{(p)}^{II}$ and that Hg_(p) is derived completely from Hg_(g)^{II}, then $\text{Hg}_{(g)}^{II}$ $\Delta^{199}\text{Hg}$ can be used to estimate $\text{Hg}_{(p)}^{II}$ $\Delta^{199}\text{Hg}$ at $t = 0$. Solving Eq. 6 for f yields an estimate for the extent of photoreduction, $\text{Hg}_{(p)}^{II} \xrightarrow{h\nu} \text{Hg}_{(g)}^0$, in the range of 46-87%.

4.3.4 MIF of ^{200}Hg and ^{204}Hg

Significant MIF of ^{200}Hg was recently reported in precipitation and $\text{Hg}^0_{(\text{g})}$ collected in the Great Lakes region of the U.S. (Gratz et al., 2010), Florida (Sherman et al, 2012) and Canada (Chen et al, 2012). Our results support the findings these authors with $\Delta^{200}\text{Hg}$ values greater than the 2SD uncertainty (0.06‰) measured in all $\text{Hg}^0_{(\text{g})}$, $\text{Hg}^{\text{II}}_{(\text{g})}$, and $\text{Hg}_{(\text{p})}$ samples, with the exception of two. Additionally, significant MIF of ^{204}Hg was also observed in most samples. Procedural replicates show that the $\Delta^{200}\text{Hg}$ and $\Delta^{204}\text{Hg}$ values measured in samples are reproducible. Furthermore, standards and procedural standards do not show significant MIF of ^{200}Hg or ^{204}Hg . MIF of ^{200}Hg and ^{204}Hg cannot arise due to the magnetic isotope effect because even Hg isotopes have no nuclear magnetic moment or nuclear spin (Buchachenko et al., 2004). The nuclear volume effect (NVE) is expected to induce slight MIF of the even Hg isotopes (Schauble, 2007). Significant MIF of ^{200}Hg measured here and in other studies combined with uncertainties in the nuclear charge radii of Hg isotopes suggests that the magnitude of NVE may not be adequately estimated at this time. It is also possible that other unidentified processes could cause MIF of ^{200}Hg and ^{204}Hg , such as photochemical self-shielding (Mead et al, 20120). However, photochemical self-shielding is expected to enrich the least abundant isotopes in the oxidized species. In this study ^{204}Hg is more anomalously enriched in the reduced species. More research is needed to elucidate the mechanisms causing MIF of the even ^{200}Hg and ^{204}Hg isotopes.

4.4 Back-Trajectory Modeling

Back-trajectories of the air masses sampled in Grand Bay, MS were estimated using the NOAA Hybrid Single Particle Lagrangian Integrated Trajectory Model (HYSPLIT V4.9) in an effort to possibly distinguish different sources of atmospheric Hg. Back-trajectories were simulated starting at a height of $\frac{1}{2}$ of the Planetary Boundary Layer height every 30 minutes for the duration of a given sample. Each back-trajectory was run for 120 hr. The set of trajectories corresponding to any given sample (or group of samples) were then subjected to a “grid-frequency” analysis, i.e., using the HYSPLIT program “TRAJFREQ”. The gridded trajectory frequency results mapped are the average fraction of the set of 120-hr back-trajectories for a given sample (or group of samples) in each grid cell (1 x 1 degree grid).

For example, Figure 4.1 illustrates the back-trajectory determined for the samples collected on April 25, 2011. The color in the grid box corresponds to the amount of time the trajectories spent in each grid box. This trajectory indicates that the air mass sampled on April 25, 2011 traveled from the Atlantic Ocean off the coast of North Carolina down around the east coast of Florida and back up the west coast off Florida before being sampled in Grand Bay, MS.

$\text{Hg}^0_{(\text{g})}$ samples were separated into two groups based on $\delta^{202}\text{Hg}$ values. $\delta^{202}\text{Hg}$ values ≤ -2 ‰ are considered low values while $\delta^{202}\text{Hg}$ values > -2 ‰ are considered high values. Back-trajectories associated with each group were then combined to form one combined frequency analysis trajectory. Interestingly, $\text{Hg}^0_{(\text{g})}$ samples displaying low $\delta^{202}\text{Hg}$ values tend to be associated with air masses that originated in the marine environment (Figure 4.2). $\text{Hg}^0_{(\text{g})}$ samples displaying high $\delta^{202}\text{Hg}$ values tend to have a larger continental component in the back-trajectories, which is seen most clearly when the trajectories are mapped on a grid with 0.1 x 0.1 degree grid cells (Figure 4.3).

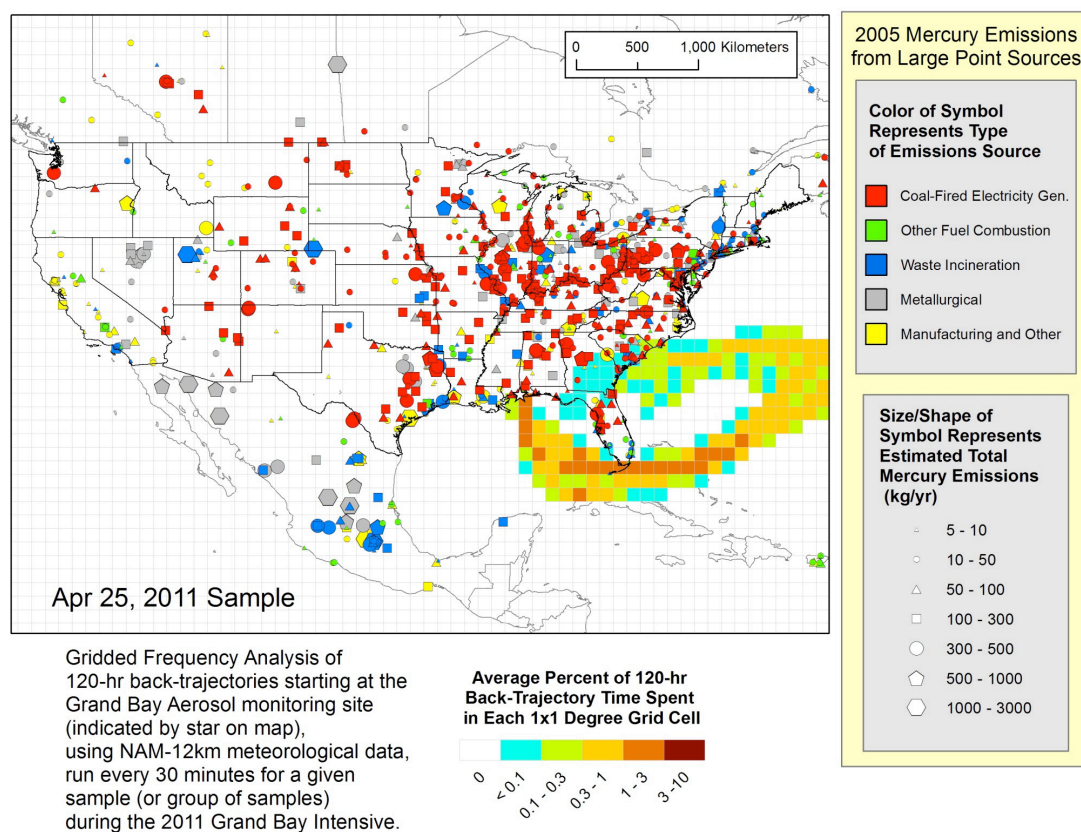


Figure 4.1: NOAA HYSPLIT back-trajectory collect for samples on April 25, 2011 (courtesy of Mark Cohen NOAA/ARL unpublished data).

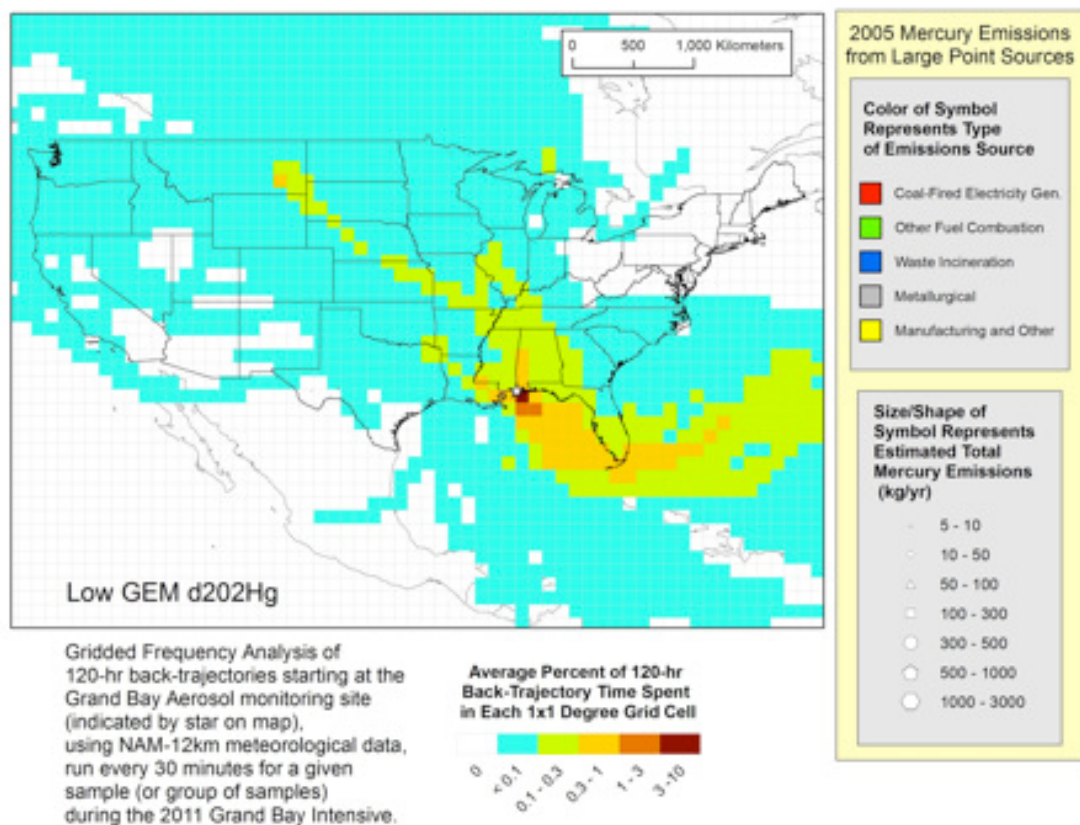


Figure 4.2: Compilation of back-trajectories on days when $\text{Hg}_{(g)}^0$ samples displayed $\delta^{202}\text{Hg}$ values $\leq -2\text{‰}$ (courtesy of Mark Cohen NOAA/ARL unpublished data).

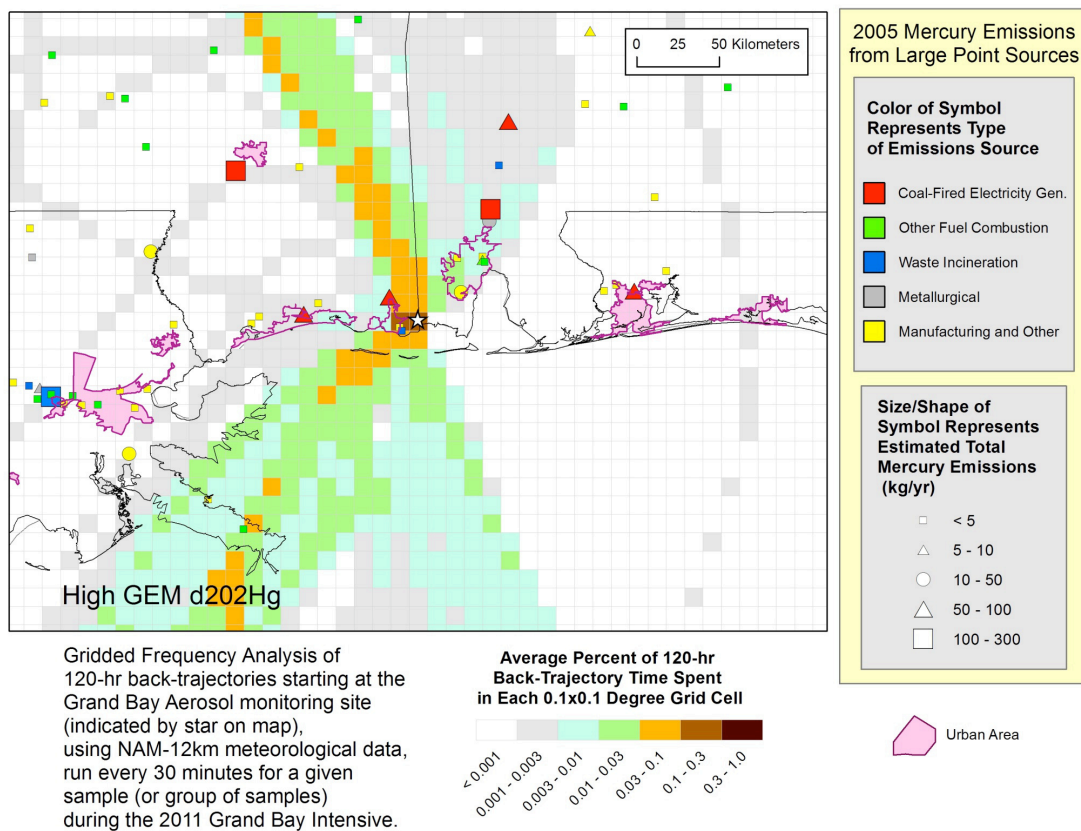


Figure 4.3: Compilation of back-trajectories on days when $\text{Hg}_{(g)}^0$ samples displayed $\delta^{202}\text{Hg}$ values $> -2\text{‰}$ (courtesy of Mark Cohen NOAA/ARL unpublished data).

CHAPTER FIVE

CONCLUSION

The isotopic composition of species-specific atmospheric Hg has been measured in a coastal environment along the northern coast of the Gulf of Mexico. $\text{Hg}^0_{(\text{g})}$, $\text{Hg}^{\text{II}}_{(\text{g})}$ compounds, and $\text{Hg}_{(\text{p})}$ were collected on gold traps, KCl treated quartz fiber filters, and untreated quartz fiber filters, respectively. All three species are isotopically distinct suggesting that isotope tracing of each species is possible.

$\text{Hg}^0_{(\text{g})}$ samples collected at Grand Bay National Estuarine Research Reserve were isotopically similar to published analysis of $\text{Hg}^0_{(\text{g})}$ at other sites and to a variety of U.S. coal deposits. However, photoreduction of $\text{Hg}^{\text{II}}_{(\text{aq})}$ in surface waters of the Gulf of Mexico could also produce $\text{Hg}^0_{(\text{g})}$ with negative mass dependent fractionation (MDF) and negative mass independent fractionation (MIF). Source attribution of atmospheric $\text{Hg}^0_{(\text{g})}$ at GB may be possible if the isotopic compositions of primary emission sources were significantly different from each other and from the global background. A diurnal variation observed in $\text{Hg}^{\text{II}}_{(\text{g})}$ and $\text{Hg}_{(\text{p})}$ concentrations suggests that the primary source of $\text{Hg}^{\text{II}}_{(\text{g})}$ and $\text{Hg}_{(\text{p})}$ at GB is the photochemical oxidation of $\text{Hg}^0_{(\text{g})}$. Disagreement between the measured fractionation factor ($\alpha_{\text{Hg}^{\text{II}}_{(\text{g})}-\text{Hg}^0_{(\text{g})}}^{202/198}$) and theoretical fractionation factors ($\alpha_{\text{HgCl}_2-\text{Hg}^0_{(\text{g})}}^{202/198}$ and $\alpha_{\text{HgBr}_2-\text{Hg}^0_{(\text{g})}}^{202/198}$) may reflect additional isotope fractionation during the conversion of $\text{Hg}^{\text{II}}_{(\text{g})}$ to $\text{Hg}_{(\text{p})}$, possibly due to diffusion of $\text{Hg}^{\text{II}}_{(\text{g})}$ into aerosols. Our observation of positive mass independent fractionation in $\text{Hg}_{(\text{p})}$ suggests that significant in-aerosol photochemical reduction of Hg^{II} has taken place.

APPENDIX 1

SAMPLE COLLECTION INFORMATION FOR THE OLF AND GB SITES

A1.1 Introduction

Appendix 1 contains the sampling information for all samples collected for Hg isotope analysis regardless if they have been analyzed or not. For each filter sample the dates, times, locations, and operating conditions of the aerosol sampler used for flow rate calculations are provided. Dates, times, and locations for the gold trap samples are also included but flow rates were not measured.

Table A.1: Sample information for KCl treated quartz fiber filters and untreated quartz fiber filters collected at the OLF site. Yellow highlighting indicates that both filter types were collected on that date and time. Dates that are not highlighted indicate that only an untreated quartz fiber filter was collected. Local time is Central Standard Time.

Site	Date Deployed	Time Deployed (local)	Date Recovered	Time Recovered (local)	Duration (hours)	Start Vacuum (0-200 inches H2O)	Stop Vacuum (0-200 inches H2O)
OLF	7/29/10	13:56	7/30/10	14:50	24.9	-	-
OLF	7/30/10	14:50	7/31/10	10:56	20.1	-	-
OLF	7/31/10	11:05	8/1/10	12:15	25.2	-	-
OLF	8/1/10	12:26	8/2/10	11:00	22.6	-	-
OLF	8/2/10	-	8/3/10	-	-	-	-
OLF	8/3/10	11:32	8/4/10	11:42	24.2	-	-
OLF	8/4/10	11:46	8/5/10	12:03	24.3	-	21.00
OLF	8/5/10	12:30	8/6/10	12:25	23.9	21.63	21.90
OLF	8/6/10	12:41	8/7/10	12:42	24.0	21.30	21.60
OLF	8/7/10	13:00	8/8/10	14:50	25.8	20.90	-
OLF	8/8/10	14:52	8/9/10	12:48	21.9	19.80	21.20
OLF	8/9/10	13:01	8/10/10	13:17	24.3	21.10	21.60
OLF	8/10/10	13:30	8/11/10	12:58	23.5	20.30	20.60
OLF	8/11/10	13:09	8/12/10	12:30	23.3	18.70	19.30
OLF	8/12/10	12:42	8/13/10	9:20	20.6	21.20	21.00
OLF	8/13/10	9:54	8/14/10	11:05	25.2	20.60	21.05
OLF	8/14/10	11:14	8/17/10	9:15	70.0	21.20	22.70
OLF	8/17/10	9:24	8/19/10	11:20	49.9	22.70	23.55
OLF	8/19/10	11:30	8/22/10	17:30	78.0	23.58	23.33
OLF	8/22/10	17:35	8/25/10	8:50	63.2	22.31	N/A
OLF	8/25/10	9:04	8/28/10	10:37	73.5	21.68	21.87
OLF	8/28/10	10:45	8/31/10	9:45	71.0	21.88	22.02
OLF	8/31/10	10:23	9/3/10	13:20	75.0	23.45	24.76
OLF	9/3/10	13:30	9/6/10	12:00	70.5	19.06	19.63
OLF	9/6/10	12:15	9/9/10	9:40	69.4	19.00	19.59
OLF	9/9/10	9:50	9/12/10	17:02	79.2	19.12	19.74
OLF	9/12/10	17:11	9/15/10	14:28	69.3	19.35	19.65
OLF	9/15/10	14:40	9/18/10	13:55	71.3	18.53	19.37
OLF	9/18/10	14:00	9/24/10	17:03	147.0	18.95	19.62
OLF	9/24/10	15:08	9/27/10	10:13	67.1	18.95	19.16
OLF	9/27/10	10:25	9/30/10	11:27	73.0	19.10	20.03
OLF	9/30/10	11:35	10/3/10	10:42	71.1	19.10	19.80
OLF	10/3/10	10:50	10/6/10	12:14	73.4	18.36	19.11
OLF	10/6/10	12:25	10/9/10	13:17	72.9	18.52	19.89
OLF	10/9/10	13:25	10/12/10	18:10	76.7	19.45	19.51
OLF	10/12/10	18:16	10/15/10	10:48	64.5	18.89	19.48
OLF	10/15/10	10:54	10/18/10	10:34	71.7	18.13	18.75
OLF	10/18/10	10:43	10/21/10	13:05	74.4	19.02	20.03
OLF	10/21/10	13:10	10/24/10	11:35	70.4	19.25	19.66
OLF	10/24/10	11:45	10/27/10	10:48	71.0	18.18	18.59
OLF	10/27/10	10:56	10/30/10	15:05	76.1	18.06	18.63
OLF	10/30/10	15:14	11/2/10	13:05	69.8	18.38	18.68
OLF	11/2/10	13:15	11/5/10	11:30	70.2	18.03	18.60
OLF	11/5/10	-	11/8/10	-	-	-	-
OLF	11/8/10	12:42	11/11/10	9:18	68.6	19.02	-
OLF	11/18/10	9:15	11/20/10	10:15	49.0	19.00	19.15
OLF	11/20/10	10:25	11/23/10	10:25	72.0	19.07	19.85
OLF	11/23/10	10:33	11/26/10	10:50	72.3	19.52	19.36
OLF	11/26/10	11:01	11/29/10	16:50	77.8	18.49	19.16
OLF	11/29/10	17:00	12/2/10	12:05	67.1	18.39	18.63
OLF	12/2/10	12:18	12/5/10	16:00	75.7	17.95	18.02
OLF	12/5/10	16:10	12/8/10	10:20	66.2	17.34	18.07
OLF	12/8/10	10:35	12/11/10	10:48	72.2	21.02	22.92
OLF	12/11/10	10:55	12/14/10	9:15	70.3	22.35	21.74
OLF	12/14/10	9:26	12/17/10	13:10	75.7	16.66	18.15
OLF	12/17/10	13:18	12/20/10	13:30	72.2	21.59	22.36

Table A.1 *continued.*

Site	Date Deployed	Time Deployed (local)	Date Recovered	Time Recovered (local)	Duration (hours)	Start Vacuum (0-200 inches H2O)	Stop Vacuum (0-200 inches H2O)
OLF	12/20/10	13:49	12/23/10	10:30	68.7	21.86	21.85
OLF	12/23/10	10:40	12/26/10	15:00	76.3	20.61	21.05
OLF	12/26/10	15:10	12/29/10	9:00	65.8	21.24	22.92
OLF	12/29/10	9:30	1/1/11	16:55	79.4	21.71	22.98
OLF	1/1/11	17:10	1/4/11	9:15	64.1	20.19	22.62
OLF	1/4/11	9:30	1/7/11	9:00	71.5	21.25	21.66
OLF	1/7/11	9:10	1/10/11	9:00	71.8	21.96	21.86
OLF	1/10/11	9:30	1/13/11	9:10	71.7	21.41	21.55
OLF	1/13/11	9:30	1/16/11	16:00	78.5	20.36	20.58
OLF	1/16/11	16:30	1/19/11	15:15	70.7	21.51	22.38
OLF	1/19/11	15:35	1/22/11	11:45	68.2	22.65	22.19
OLF	1/22/11	12:00	1/25/11	14:16	74.3	20.91	22.05
OLF	1/25/11	14:30	1/28/11	15:00	72.5	21.85	22.95
OLF	1/28/11	15:30	1/31/11	8:30	65.0	20.66	21.86
OLF	1/31/11	8:40	2/3/11	9:15	72.6	21.22	20.91
OLF	2/3/11	9:30	2/6/11	13:15	75.8	20.88	22.21
OLF	2/6/11	12:44	2/9/11	15:30	74.8	22.33	22.30
OLF	2/9/11	17:40	2/15/11	15:10	141.5	20.77	22.47
OLF	2/15/11	15:20	2/18/11	18:10	74.8	20.03	21.81
OLF	2/18/11	18:30	2/21/11	10:35	64.1	21.23	22.33
OLF	2/21/11	10:45	2/24/11	12:35	73.8	19.84	20.37
OLF	2/24/11	12:45	2/27/11	13:30	72.8	19.58	20.56
OLF	2/27/11	13:45	3/2/11	9:30	67.8	21.79	22.68
OLF	3/2/11	15:36	3/5/11	8:00	64.4	19.65	20.38
OLF	3/5/11	8:15	3/8/11	11:00	74.8	18.35	19.42
OLF	3/8/11	11:30	3/11/11	11:40	72.2	19.45	19.99
OLF	3/11/11	12:00	3/14/11	9:30	69.5	16.67	20.27
OLF	3/14/11	9:45	3/17/11	15:45	78.0	19.52	20.71
OLF	3/17/11	16:00	3/20/11	16:30	72.5	20.09	20.86
OLF	3/20/11	16:45	3/23/11	9:10	64.4	19.96	20.24
OLF	3/23/11	9:30	3/26/11	15:30	78.0	19.74	20.59
OLF	3/26/11	15:45	3/29/11	12:30	68.8	19.47	19.92
OLF	3/29/11	12:45	4/1/11	8:15	67.5	18.67	19.47
OLF	4/1/11	8:30	4/4/11	12:15	75.8	19.74	20.73
OLF	4/4/11	12:30	4/7/11	9:30	69.0	19.82	20.18
OLF	4/7/11	9:45	4/10/11	12:30	74.8	19.79	20.48
OLF	4/10/11	12:45	4/13/11	10:00	69.2	19.75	20.68
OLF	4/13/11	10:15	4/16/11	13:05	74.8	19.91	20.62
OLF	4/16/11	13:20	4/19/11	9:35	68.3	20.24	20.87
OLF	4/19/11	10:45	4/20/11	9:40	22.9	37.00	39.50
OLF	4/20/11	9:50	4/21/11	9:50	24.0	38.80	44.80
OLF	4/21/11	9:53	4/22/11	9:30	23.6	37.10	49.20
OLF	4/22/11	9:35	4/23/11	10:30	24.9	37.20	45.70
OLF	4/23/11	10:36	4/24/11	11:45	25.2	38.10	45.40
OLF	4/24/11	11:50	4/25/11	10:28	22.6	40.00	43.40
OLF	4/25/11	10:33	4/26/11	10:37	24.1	38.70	45.20
OLF	4/26/11	10:42	4/28/11	9:40	47.0	40.80	50.30
OLF	4/28/11	9:45	4/29/11	10:30	24.8	37.50	40.00
OLF	4/29/11	10:35	4/30/11	9:50	23.3	38.90	39.90
OLF	4/30/11	9:53	5/1/11	11:15	25.4	40.50	41.20
OLF	5/1/11	11:18	5/2/11	10:10	22.9	14.80	16.40
OLF	5/2/11	10:15	5/3/11	10:10	23.9	35.00	46.00
OLF	5/3/11	10:16	5/4/11	9:53	23.6	41.50	43.90
OLF	5/4/11	9:55	5/5/11	10:07	24.2	40.10	42.20
OLF	5/5/11	10:10	5/6/11	10:22	24.2	39.20	42.50
OLF	5/6/11	10:24	5/7/11	9:40	23.3	40.00	42.20
OLF	5/7/11	9:42	5/8/11	10:02	24.3	40.60	42.80
OLF	5/8/11	10:05	5/9/11	9:58	23.9	40.90	46.30
OLF	5/9/11	10:02	5/10/11	12:18	26.3	34.60	41.60

Table A.1 *continued.*

Site	Date Deployed	Time Deployed (local)	Date Recovered	Time Recovered (local)	Duration (hours)	Start Vacuum (0-200 inches H2O)	Stop Vacuum (0-200 inches H2O)
OLF	5/10/11	12:25	6/22/11	13:30	1033.1	20.00	28.65
OLF	6/22/11	13:30	6/24/11	10:05	44.6	20.45	20.95
OLF	6/24/11	10:15	7/9/11	17:00	366.8	19.78	20.61
OLF	7/9/11	17:30	7/11/11	9:30	40.0	18.87	19.68
OLF	7/12/11	9:45	7/15/11	10:45	73.0	18.95	19.72
OLF	7/15/11	11:00	7/18/11	11:00	72.0	19.11	19.56
OLF	7/18/11	11:15	7/21/11	10:20	71.1	21.45	22.44
OLF	7/21/11	10:40	7/24/11	14:00	75.3	17.69	19.73
OLF	7/24/11	14:30	7/27/11	11:15	68.8	19.52	19.26
OLF	7/27/11	11:20	8/2/11	10:58	143.6	19.11	20.55
OLF	8/2/11	11:20	8/8/11	13:45	146.4	19.27	20.78
OLF	8/8/11	13:00	8/14/11	13:45	144.8	19.94	20.34
OLF	8/14/11	14:00	8/17/11	9:25	67.4	19.14	19.83
OLF	8/17/11	9:35	8/23/11	10:15	144.7	19.29	20.45
OLF	8/23/11	10:30	8/26/11	8:30	70.0	19.51	19.83
OLF	8/26/11	8:45	8/29/11	8:40	71.9	19.17	20.25
OLF	8/29/11	8:55	9/1/11	8:50	71.9	19.25	19.81
OLF	9/1/11	9:05	9/7/11	9:30	144.4	19.03	19.27
OLF	9/7/11	9:40	9/10/11	10:15	72.6	19.17	20.41
OLF	9/10/11	10:30	9/13/11	9:30	71.0	19.75	20.28
OLF	9/13/11	9:42	9/16/11	9:30	71.8	19.38	19.31
OLF	9/16/11	9:40	9/19/11	9:30	71.8	19.01	19.77
OLF	9/19/11	9:18	9/22/11	9:50	72.5	19.18	20.20
OLF	9/22/11	7:40	9/25/11	15:40	80.0	21.32	21.98
OLF	9/25/11	15:48	9/28/11	9:10	65.4	20.09	20.82
OLF	9/28/11	9:30	10/1/11	8:45	71.3	21.25	20.85
OLF	10/1/11	9:00	10/4/11	13:00	76.0	19.82	21.70
OLF	10/4/11	13:15	10/7/11	10:10	68.9	21.80	22.16
OLF	10/7/11	10:20	10/10/11	8:50	70.5	21.25	21.52
OLF	10/10/11	9:00	10/13/11	9:00	72.0	37.05	45.36
OLF	10/13/11	9:15	10/16/11	16:45	79.5	32.89	38.46
OLF	10/16/11	17:00	10/19/11	9:15	64.2	38.93	45.18
OLF	10/19/11	9:30	10/25/11	12:15	146.7	34.65	38.19
OLF	10/25/11	12:30	10/28/11	9:15	68.7	38.08	41.82
OLF	10/28/11	9:30	10/31/11	13:20	75.8	37.67	38.42
OLF	10/31/11	13:30	11/3/11	9:10	67.7	38.11	40.91
OLF	11/3/11	9:20	11/6/11	16:00	78.7	37.33	39.74
OLF	11/6/11	16:20	11/9/11	12:40	68.3	36.17	39.32
OLF	11/9/11	12:50	11/12/11	16:15	75.4	37.23	39.67
OLF	11/12/11	16:30	11/15/11	13:40	69.2	36.33	42.28
OLF	11/15/11	13:55	11/18/11	10:20	68.4	37.52	41.92
OLF	11/18/11	10:40	11/21/11	9:30	70.8	37.79	43.35
OLF	11/21/11	9:45	11/24/11	9:30	71.8	37.12	43.57
OLF	11/23/11	9:35	11/27/11	17:00	103.4	36.11	72.78
OLF	11/27/11	17:15	11/30/11	10:30	65.3	35.98	39.23
OLF	11/30/11	10:45	12/3/11	15:40	76.9	35.72	37.72
OLF	12/3/11	15:50	12/6/11	9:10	65.3	37.69	74.02
OLF	12/6/11	9:30	12/9/11	8:45	71.3	37.41	37.42
OLF	12/9/11	9:00	12/12/11	13:00	76.0	35.63	36.91
OLF	12/12/11	13:15	12/16/11	13:35	96.3	37.16	40.98
OLF	12/16/11	13:40	12/21/11	9:20	115.7	37.59	52.17
OLF	12/21/11	9:35	12/24/11	15:15	77.7	45.96	53.84
OLF	12/24/11	15:20	12/27/11	9:45	66.4	46.13	73.43
OLF	12/27/11	9:55	12/30/11	8:55	71.0	37.18	46.71
OLF	12/30/11	9:05	1/2/12	9:50	72.8	44.18	54.07
OLF	1/2/12	10:00	1/5/12	12:50	74.8	43.87	46.90
OLF	1/5/12	13:00	1/8/12	14:50	73.8	45.90	49.01
OLF	1/8/12	15:00	1/11/12	10:55	67.9	45.75	66.86
OLF	1/11/12	11:05	1/14/12	13:15	74.2	45.77	48.79
OLF	1/14/12	13:25	1/17/12	9:20	67.9	44.54	49.68
OLF	1/17/12	9:30	1/20/12	9:15	71.7	44.71	54.04

Table A.2: Sample information for KCl treated quartz fiber filters and untreated quartz fiber filters collected at the GB site. Yellow highlighting indicates that both filter types were collected on that date and time. Dates that are not highlighted indicate that only an untreated quartz fiber filter was collected. Local time is Central Standard Time.

Site	Date Deployed	Time Deployed (local)	Date Recovered	Time Recovered (local)	Duration (hours)	Start Pressure (0-200 inches H2O)	Start Pressure (P0-200 inches H2O)
Grand Bay	7/30/10	11:40	7/31/10	14:39	27.0	4.25	4.45
Grand Bay	7/31/10	15:05	8/1/10	15:46	24.7	4.48	4.4
Grand Bay	8/1/10	15:55	8/2/10	14:45	22.8	4.7	4.75
Grand Bay	8/2/10	14:55	8/3/10	13:55	23.0	4.64	4.8
Grand Bay	8/3/10	13:45	8/4/10	14:54	25.2	4.85	4.5
Grand Bay	8/4/10	14:58	8/5/10	14:30	23.5	4.6	4.41
Grand Bay	8/5/10	14:45	8/6/10	16:15	25.5	4.52	4.55
Grand Bay	8/6/10	16:28	8/7/10	15:36	23.1	4.9	4.6
Grand Bay	8/7/10	15:52	8/8/10	19:36	27.7	4.51	4.7
Grand Bay	8/8/10	19:42	8/9/10	18:55	23.2	5.12	4.98
Grand Bay	8/9/10	19:10	8/10/10	18:34	23.4	5.1	5.04
Grand Bay	8/10/10	18:44	8/11/10	14:55	20.2	5.05	4.65
Grand Bay	8/11/10	15:05	8/12/10	14:05	23.0	4.59	4.7
Grand Bay	8/12/10	14:15	8/13/10	13:35	23.3	4.72	4.58
Grand Bay	8/13/10	13:50	8/14/10	14:00	24.2	4.65	4.85
Grand Bay	4/18/11	17:30	4/19/11	17:15	23.8	39.0	42.3
Grand Bay	4/19/11	17:20	4/20/11	17:20	24.0	40.0	46.7
Grand Bay	4/20/11	17:25	4/21/11	15:12	21.8	40.2	44.4
Grand Bay	4/21/11	15:17	4/22/11	13:40	22.4	39.2	41.8
Grand Bay	4/22/11	13:45	4/23/11	12:00	22.3	41.5	43.9
Grand Bay	4/23/11	12:03	4/24/11	13:13	25.2	40.2	42.1
Grand Bay	4/24/11	13:16	4/25/11	12:31	23.3	39.5	43.0
Grand Bay	4/25/11	12:35	4/26/11	12:23	23.8	39.0	48.8
Grand Bay	4/26/11	12:33	4/28/11	12:07	47.6	41.2	44.6
Grand Bay	4/28/11	12:10	4/29/11	12:15	24.1	40.3	40.4
Grand Bay	4/29/11	12:20	4/30/11	11:35	23.3	37.2	39.8
Grand Bay	4/30/11	11:40	5/1/11	9:32	21.9	40.1	41.0
Grand Bay	5/1/11	9:36	5/2/11	11:52	26.3	38.5	38.0
Grand Bay	5/2/11	11:57	5/3/11	12:00	24.0	41.0	45.9
Grand Bay	5/3/11	12:05	5/4/11	11:20	23.3	41.8	43.6
Grand Bay	5/4/11	11:26	5/5/11	11:40	24.2	41.1	41.7
Grand Bay	5/5/11	11:45	5/6/11	12:10	24.4	42.0	43.2
Grand Bay	5/6/11	12:15	5/7/11	11:10	22.9	42.1	43.4
Grand Bay	5/7/11	11:15	5/8/11	8:22	21.1	43.0	44.0
Grand Bay	5/8/11	8:23	5/9/11	11:22	27.0	40.1	41.8

Table A.3: Sample information for Au traps collected at the both the Grand Bay and OLF sites. Local time is Central Standard Time. Flow rates were not monitored for Au trap samples.

Site	Date Deployed	Time Deployed (local)	Date Recovered	Time Recovered (local)	Duration (hours)
Grand Bay	4/19/11	17:45	4/20/11	17:27	23.7
Grand Bay	4/20/11	17:35	4/21/11	15:20	21.8
Grand Bay	4/21/11	15:25	4/22/11	13:45	22.3
Grand Bay	4/22/11	14:00	4/23/11	12:04	22.1
Grand Bay	4/23/11	12:04	4/24/11	13:16	25.2
Grand Bay	4/24/11	13:17	4/25/11	12:40	23.4
Grand Bay	4/25/11	12:35	4/26/11	12:23	23.8
Grand Bay	4/26/11	14:00	4/28/11	12:20	46.3
Grand Bay	4/28/11	12:25	4/29/11	12:30	24.1
Grand Bay	4/29/11	13:00	4/30/11	11:45	22.8
Grand Bay	4/30/11	11:45	5/1/11	9:37	21.9
Grand Bay	5/1/11	9:37	5/2/11	11:55	26.3
Grand Bay	5/2/11	11:55	5/3/11	12:05	24.2
Grand Bay	5/3/11	13:00	5/4/11	11:25	22.4
Grand Bay	5/4/11	11:25	5/5/11	11:44	24.3
Grand Bay	5/5/11	11:45	5/6/11	12:13	24.5
Grand Bay	5/6/11	12:13	5/7/11	11:13	23.0
Grand Bay	5/7/11	11:14	5/8/11	8:25	21.2
Grand Bay	5/8/11	8:25	5/9/11	11:24	27.0
OLF	4/19/11	10:35	4/25/11	10:37	144.0
OLF	4/19/11	10:35	4/25/11	10:37	144.0
OLF	4/25/11	10:46	5/2/11	10:23	167.6
OLF	4/25/11	10:46	5/2/11	10:23	167.6
OLF	5/2/11	10:24	5/10/11	12:08	193.7
OLF	5/2/11	10:24	5/10/11	12:08	193.7

REFERENCES

- Bergquist, B.A. and Blum, J.D., 2007. Mass-dependent and mass-independent fractionation of Hg isotopes by photoreduction in aquatic systems. *Science* 318, 417-420.
- Biswas, A., Blum, J.D., Bergquist, B.A., Keeler, G.J., Xie, Z., 2008. Natural mercury isotope variation in coal deposits and organic soils. *Environmental Science and Technology* 42, 8303-8309.
- Buchachenko, A.L., Kouznetsov, D.A., Shishkov, A.V., 2004. Spin biochemistry: magnetic isotope effect in the reaction of creatine kinase with CH_3HgCl . *Journal of Physical Chemistry A* 108, 707-710.
- Caffrey, J.M., Landing, W.M., Nolek, S.D., Gosnell, K., Bagui, S.S. Bagui, S.C., 2010. Atmospheric deposition of mercury and major ions to the Pensacola Bay (Florida) watershed: spatial, seasonal, and inter-annual variability. *Atmospheric Chemistry and Physics Discussions* 10, 4593-4616.
- Capri, A., 1996. Mercury from combustion sources: a review of the chemical species emitted and their transport in the atmosphere. *Water, Air, Soil Pollution* 98, 241-254.
- Carignan, J., Estrade, N., Sonke, J.E., Donard, O.F.X., 2009. Odd isotope deficits in atmospheric mercury measured in lichens. *Environmental Science and Technology* 43, 5560-5564.
- Chen, J., Hintelmann, H., Feng, X., Dimock, B., Unusual fractionation of both odd and even mercury isotopes in precipitation from Peterborough, ON., Canada, *Geochimica et Cosmochimica Acta* (2012), doi: <http://dx.doi.org/10.1016/j.gca.2012.05.005>
- Das, R., Salters, V.J.M., Odom, L., 2009. A case for in vivo mass-independent fractionation of mercury isotopes in fish. *Geochemistry, Geophysics, Geosystems* 20, Q11012.
- Edgerton, E.S., Hartsell, B.E., Jansen, J.J., 2006. Mercury speciation in coal-fired power plant plumes observed at three surface sites in the southeastern U.S. *Environmental Science and Technology* 40, 4563-4570.
- Epov, V.N., 2011. Magnetic isotope effect and theory of atomic orbital hybridization to predict a mechanism of chemical exchange reactions. *Physical Chemistry and Chemical Physics* 13, 13222-13231.
- Estrade, N., Carignan, J., Sonke, J.E., Donard, O.F.X., 2009. Mercury isotope fractionation during liquid-vapor evaporation experiments. *Geochimica et Cosmochimica Acta* 73, 2693-2711.
- Estrade, N., Carignan, J., Sonke, J.E., Donard, O.F.X., 2010. Measuring Hg isotopes in bio-geo-environmental reference materials. *Geostandard and Geoanalysis Research* 34 (1), 79-93.

- Fitzgerald, W.F., Engstrom, D.R., Lamborg, C.H., Tseng, C.M., Balcom, P.H., Hammerschmidt, C.R., 2005. Modern and historic atmospheric mercury fluxes in northern Alaska: global sources and Arctic depletion. *Environmental Science and Technology* 39, 557-568.
- Ghosh, S., Xu, Y., Humayun, M., Odom, L., 2008. Mass-independent fractionation of mercury isotopes in the environment. *Geochemistry, Geophysics, Geosystems* 9 (3), Q03004.
- Gratz L.E., Keeler, G.J., Blum, J.D., Sherman, L.S., 2010. Isotopic composition and fractionation of mercury in great lakes precipitation and ambient air. *Environmental Science and Technology* 44, 7764-7770.
- Guentzel, J.L., Landing, W.L., Gill, G.A., Pollman, C.D., 2001. Processes influencing rainfall deposition of mercury in Florida. *Environmental Science and Technology* 35, 863-873.
- Holmes, C.D., Jacob, D.J., Mason, R.P., Jaffe, D.A., 2009. Sources and deposition of reactive gaseous mercury in the marine atmosphere. *Atmospheric Environment* 43, 2278-2285.
- Jackson, T.A., Whittle, D.M., Evans, M.S., Muir, D.G., 2008. Evidence for mass-independent and mass dependent fractionation of the stable isotopes of mercury by natural process in aquatic ecosystems. *Applied Geochemistry* 23, 547-571.
- Kritee, K., Blum, J.D., Johnson, M.W., Bergquist, B.A., Barkay, T., 2007. Mercury stable isotope fractionation during reduction of Hg(II) to Hg(0) by mercury resistant microorganisms. *Environmental Science and Technology* 41, 1889-1895.
- Kritee, K., Blum, J.D., Barkay, T., 2008. Mercury stable isotope fractionation during reduction of Hg(II) by different microbial pathways. *Environmental Science and Technology* 42, 9171-9177.
- Kritee, K., Barkay, T., Blum, J.D., 2009. Mass dependent stable isotope fractionation of mercury during mer mediated microbial degradation of monomethylmercury. *Geochimica et Cosmochimica Acta* 73, 1285-1296.
- Laffont, L., Sonke, J.E., Maurice, L., Hintelmann, H., Sanchez-Baccarez, Y., Perez, T., Behra, P., 2009. Anomalous mercury isotopic compositions of fish and human hair in the Bolivian Amazon. *Environmental Science and Technology* 43, 8985-8990.
- Landis, M.S., Keeler, G.J., 2002. Atmospheric mercury deposition to Lake Michigan during the Lake Michigan Mass Balance Study. *Environmental Science and Technology* 36, 4518-4524.
- Landis, M.S., Stevens, R.K., Schaedlich, F., Prestbo, E.M., 2002. Development and characterization of an annular denuder methodology for the measurement of divalent inorganic reactive gaseous mercury in ambient air. *Environmental Science and Technology* 36, 3000-3009.
- Landis, M.S., Lynam, M.M., Stevens, R.K., 2005. The monitoring and modeling of mercury species in support of local, regional and global modeling, in *Dynamics of Mercury*

- Pollution on Regional and Global Scales*, edited by N. Pirrone and K.R. Mahaffey, pp. 123-151, Springer, New York.
- Laurier, F.J.G., Mason, R.P., Whalin, L., 2003. Reactive gaseous mercury formation in the North Pacific Ocean's marine boundary layer: A potential role of halogen chemistry. *Journal of Geophysical Research* 108, 4529.
- Lin, C.J., Pehkomen, S.O., 1999. The chemistry of atmospheric mercury: a review. *Atmospheric Environment* 33, 2067-2079.
- Lindberg, S.E., Brooks, S., Lin, C.-J., Scott, K.J., Landis, M.S., Stevens, R.K., Goodsite, M., Richter, A., 2002. Dynamic oxidation of gaseous mercury in the Arctic troposphere at polar sunrise. *Environmental Science and Technology* 36, 1245-1256.
- Lindberg S., Bullock, R., Ebinghaus, R., Engstrom, D., Feng, X., Fitzgerald, W., Pirrone, N., Prestbo, E., Seigneur, C., 2007. A synthesis of progress and uncertainties in attributing the sources of mercury in deposition. *Ambio* 36, 19-32.
- Liu, B., Keeler, G.J., Dvonch, T., Barres, J.A., Lynam, M.M., Marsik, F.J., Morgan, J.T., 2010. Urban-rural differences in atmospheric mercury speciation. *Atmospheric Environment* 44, 2013-2023.
- Malcom, E.G., Keeler, G.J., Evidence for a sampling artifact for particulate-phase mercury in the marine atmosphere. *Atmospheric Environment* 41, 3352-3359.
- Mason, R.P., Sheu, G.R., 2002. Role of the ocean in the global mercury cycle. *Global Biogeochemical Cycles* 16, 1093.
- Mead, C.; Anbar, A. D.; Johnson, T. M. Mass-independent fractionation of Hg isotopes resulting from photochemical self shielding; Goldschmidt: Knoxville, TN, 2010.
- Obrist, D., Tas, E., Peleg, M., Matveev, V., Faïn, X., Asaf, D., Luria, M., 2010. Bromine-induced oxidation of mercury in the mid-latitude atmosphere. *Nature* 4, 22-26.
- Pacyna, E.G., Pacyna, J.M., Sundseth, K., Munthe, J., Kindbom, K., Wilson, S., Steenhuisen, F., Maxson, P., 2010. Global emission of mercury to the atmosphere from anthropogenic sources in 2005 and projections to 2020. *Atmospheric Environment* 44, 2487-2499.
- Pirrone, N., Costa, P., Pacyna, J.M., Ferrara, R., 2001. Mercury emissions to the atmosphere from natural and anthropogenic sources in the Mediterranean region. *Atmospheric Environment* 35, 2997-3006.
- Pirrone, N., Cinnirella, S., Feng, X., Finkelman, R.B., Friedli, H.R., Leaner, J., Mason, R., Mukherjee, A.B., Stracher, G.B., Streets, D.G., Telmer, K., 2010. Global mercury emissions to the atmosphere from anthropogenic and natural sources. *Atmospheric Chemistry and Physics Discussions* 10, 4719-4752.

- Rutter, A.P., Hanfor, K.L., Zwers, J.T., Perillo-Nicholas, A.L., Schauer, J.J., Olson, M.L., 2008. Evaluation of an offline method for the analysis of atmospheric reactive gaseous mercury and particulate mercury. *Journal of the Air & Waste Management Association* 58, 377-383.
- Schauble, E.A., 2007. Role of nuclear volume in driving equilibrium isotope fractionation of mercury, thallium, and other very heavy elements. *Geochimica et Cosmochimica Acta* 71, 2170-2189.
- Schroeder, W.H., Munthe, J., 1998. Atmospheric mercury-an overview. *Atmospheric Environment* 32 (5), 809-822.
- Selin, N.E., 2009. Global biogeochemical cycling of mercury: a review. *Annual Review of Environment and Resources* 34, 43-63.
- Sherman, L.S., Blum, J.D., Johnson, K.P., Keeler, G.J., Barres, J.A., Douglas, T.A., 2010. Mass-independent fractionation of mercury isotopes in Arctic snow driven by sunlight. *Nature Geoscience* 3, 173-177.
- Sherman, L.S., Blum, J.D., Keeler, J.G., Demers, J.D., Dvornch, J.T., 2012. Investigation of local mercury deposition from a coal-fired power plant using mercury isotopes. *Environmental Science and Technology* 46, 382-390.
- Smith, C.N., Kesler, E., Klaue, B., Blum, J.D., 2005. Mercury isotope fractionation in fossil hydrothermal systems. *Geology* 33 (10), 825-828.
- Sonke, J.E., 2011. A global model of mass independent mercury stable isotope fractionation. *Geochimica et Cosmochimica Acta* 75, 4577-4590.
- Sonke, J.E., Schaefer, J., Chmeleff, J., Audry, S., Blanc, G., Dupré, B., 2010. Sedimentary mercury stable isotope records of atmospheric and riverine pollution from two major European heavy metal refineries. *Chemical Geology* 297, 90-100.
- Sprovieri, F., Pirrone, N., Hedgecock, I.M., Landis, M.S., Stevens, R.K., 2002. Intensive atmospheric mercury measurements at Terra Nova Bay in Antarctica during November and December 2000. *Journal of Geophysical Research* 107, 4722.
- Strode, S.A., Jaeglé, L., Selin, N.E., Jacob, D.J., Park, R.J., Yantosca, R.M., Mason, R.P., Slemr, F., 2007. Air-sea exchange in the global mercury cycle. *Global Biogeochemical Cycles* 21, GB1017.
- Subir, M., Ariya, P.A., Dastoor, A.P., 2011. A review of uncertainties in atmospheric modeling of mercury chemistry I. Uncertainties in existing kinetic parameters - Fundamental limitations and the importance of heterogeneous chemistry. *Atmospheric Environment* 45, 5664-5676.

- U.S. Environmental Protection Agency. *Mercury Study Report to Congress*; EPA-452/R-97-003; U.S. EPA Office of Air Quality Planning and Standards, Office of Research and Development: Washington DC, 1997; Vol. 2.
- Wiederhold, J.G., Cramer, C.J., Daniel, K., Infante, I., Bourdon, B., Kretzchmar, R., 2010. Equilibrium mercury isotope fractionation between dissolved Hg(II) species and thiol-bound Hg. *Environmental Science and Technology* 44, 4191-4197.
- Yin, R., Feng, X., Shi, W., 2010. Application of the stable-isotope system to the study of sources and fate of Hg in the environment: A review. *Applied Geochemistry* 25, 1467-1477.
- Zambardi, T., Sonke, J.E., Toutain, J.P., Sortino, F., Shinohara, H., 2009. Mercury emissions and stable isotopic compositions at Vulcano Island (Italy). *Earth and Planetary Science Letters* 277, 236-243.
- Zheng, W., Foucher, D., Hintelmann, H., 2007. Mercury isotope fractionation during volatilization of Hg(0) from solution into the gas phase. *Journal of Analytical Atomic Spectrometry* 22, 1097-1104.
- Zheng, W., Hintelmann, H., 2009. Mercury isotope fractionation during photoreduction in natural waters is controlled by its Hg/DOC ratio. *Geochimica et Cosmochimica Acta* 73, 6704-6715.
- Zheng, W., Hintelmann, H., 2010a. Isotope fractionation of mercury during its photochemical reduction by low-molecular weight organic compounds. *Journal of Physical Chemistry A* 114, 4246-4253.
- Zheng, W., Hintelmann, H., 2010b. Nuclear field shift effect in isotope fractionation of mercury during abiotic reduction in the absence of light. *Journal of Physical Chemistry A* 114, 4238-4245.

BIOGRAPHICAL SKETCH

Personal Data

Born: March 1, 1986, Columbia, South Carolina

Education

B. Sc.: Chemistry and Marine Science 2008 University of South Carolina

M. Sc.: Chemical Oceanography 2012 Florida State University

Publications

Rolison, J.M., Landing, W.M., Luke, W., 2012. Isotopic composition of species-specific atmospheric Hg in a coastal environment. *Chemical Geology* (in revision).

Conference Presentations

Rolison, J.M. and Landing, W.M. Isotopic composition of atmospheric mercury along the northern coast of the Gulf of Mexico. 10th International Conference on Mercury as a Global Pollutant. Halifax, Nova Scotia, Canada. July 23-29, 2011.